Journal of Building Engineering 50 (2022) 104196

Contents lists available at ScienceDirect

Journal of Building Engineering

journal homepage: www.elsevier.com/locate/jobe

Damage index model and hysteretic viscous damping of masonry infill walls subjected to out-of-plane loadings

André Furtado [a,*], Hugo Rodrigues [b], António Arêde [a], Graça Vasconcelos [c], Maria Teresa de Risi [d]

[a] CONSTRUCT-LESE, Department of Civil Engineering, Faculty of Engineering of the University of Porto, Portugal
[b] RISCO, Department of Civil Engineering, University of Aveiro, Portugal
[c] ISISE, Department of Civil Engineering, University of Minho, Portugal
[d] Università degli Studi di Napoli Federico II, Italy

ARTICLE INFO

Keywords:
Masonry infill walls
Out-of-plane behaviour
Experimental testing
Damage state
Damage index
Normalized energy dissipation
Viscous damping

ABSTRACT

The definition of damage states for structural and non-structural elements is necessary to support the seismic vulnerability analyses and identify the most vulnerable elements that need to be retrofitted. The studies related to masonry infill walls focused on multiple experimental studies to characterize their in-plane and/or out-of-plane (OOP) behaviour. Some codes have already proposed damage states for masonry infill walls only under in-plane loadings. Also, the study of the normalized energy dissipation and the hysteretic viscous damping when subjected to OOP loadings were not explored. It is recognized that the OOP behaviour of masonry infill walls is still nowadays a topic needing further investigations. The main objective of this work is to propose damage index for infill walls under to pure OOP seismic loadings. For that, a detailed analysis of the damage observed in masonry infill walls tested under pure OOP loadings was performed. The damage observed in masonry infill walls made with different masonry units, with and without openings, is carefully detailed. After that, a pilot damage index model is proposed for masonry infill walls made of hollow clay horizontal brick units. The third objective of this work was the assessment and discussion of their normalized energy dissipation capacity and their hysteretic viscous damping. Some analytical formulations were proposed to estimate these parameters. A database containing thirteen OOP tests performed by three different authors was used to achieve these goals.

1. Introduction

Several post-earthquake survey damage assessment reports recognize that the masonry infill walls' Out-Of-Plane (OOP) seismic performance was responsible for multiple collapses, casualties, and economic losses [1–3]. Calvi and Bolognini [4] concluded that the damage state of the infill walls plays an essential role in the definition of damage states of Reinforced Concrete (RC). The authors justified this sentence by saying that the infill walls cannot accommodate large deformations without damaging or collapsing. For example, in well-designed RC frames according to recent seismic standards (e.g. Eurocode 8), the walls can be severely damaged or even collapsed before the RC frame is damaged.

Generally, in common practice, attention is paid only to defining damage states of RC structural members, neglecting the fragile In-

* Corresponding author.
E-mail address: afurtado@fe.up.pt (A. Furtado).

https://doi.org/10.1016/j.jobe.2022.104196
Received 20 August 2021; Received in revised form 2 February 2022; Accepted 7 February 2022
Available online 16 February 2022

Plane (IP) and OOP seismic behaviour of the walls and their seismic vulnerability. Due to the low capacity for reaching high deformation levels without damaging, the infill walls' collapse can occur before the significant deterioration of the RC structure, which implies enormous danger for human life. There is a tremendous need to investigate their OOP seismic behaviour more profoundly.

Based on this motivation, several research works have been developed to assess the masonry infill walls seismic behaviour through experimental testing. The experimental works available in the literature are divided into two approaches: i) the IP testing of infilled RC specimens [5]; and the OOP testing of infill walls surrounded by RC elements (i.e. RC frame) [6,7]. Concerning the IP testing of the infilled RC frames, the authors investigated the infill walls' impact on the lateral response of RC frames designed with low or high seismic demands. The effect of the openings, masonry units and strengthening was also the focus of multiple tests [4,8]. From those studies, it was concluded that the presence of the infill walls increases the lateral stiffness, strength and energy dissipation of the frame. However, shear failure of RC elements can also occur due to the infill walls and their openings (i.e. development of short-column mechanism) [9–11].

Variables such as masonry unit type, openings (area and disposition) and the envelope RC frame seismic design can have an important influence on the response of the wall when subjected to IP seismic loadings [12–14].

When the infill walls are subjected to OOP demand, their response becomes much more complex. It depends on several variables such as previous damage due to IP loadings, slenderness, panel support condition, aspect ratio, masonry units, openings, axial load, and workmanship [15–19], among others.

The main cause of the OOP collapse is the IP-OOP interaction, which increases the OOP vulnerability. First, Angel, et al. [20] observed an increase in the reduction of the OOP strength when the wall is subjected to greater IP drift demands. Later, Di Domenico et al. [21] investigated the effect of three levels of previous IP drift demands (light, medium and high) on the OOP strength capacity of infill walls with two different slendernesses ratios (i.e. height/thickness). From the tests, it was again observed that the wall OOP strength reduction is higher when the it is subjected to larger IP seismic demands. Nonetheless, the authors do not find a specific relationship between the slenderness and the IP-OOP strength interaction. More recently, Ricci, et al. [22] concluded that the collapse PGA of infills is significantly overestimated if the IP/OOP interaction is neglected. The authors also concluded that seismic displacement demand acting on the building structure might be highly underestimated if the IP/OOP interaction effects are neglected.

Different strategies are being proposed and validated to prevent the walls OOP collapse. The use of textile-reinforced mortar for strengthening the infill walls has been studied by Minotto et al. [23], Sagar, et al. [24] and De Risi et al. [25]. They concluded that this technique could be very effective to prevent the OOP collapse if the adequate mechanical connection of the strengthening material to the envelope RC frame is ensured. When the retrofitting is performed without effective anchorage of the strengthening material to the RC frame, the wall may experience premature failure. More information concerning other retrofitting techniques to prevent the walls OOP collapse can be found in Ref. [26].

Regarding the behaviour of masonry infill walls under pure OOP seismic loads, Dawe and Seah [27] started the first set of experimental tests, which concluded that the OOP strength is due mainly to the flexural mechanism before developing the first crack. After the first crack forms, the arching mechanism provides the OOP strength, and the walls become more flexible. The authors also observed that a panel with all four borders constrained have 5.5 times higher OOP strength when compared to panels with three edges constrained. Later, Angel, et al. [20] investigated the effect of IP cracking, deterioration in the frame-infill boundary, gravity load and tensile bond, however not provide many details concerning the damage evolution.

Di Domenico et al. [28] observed an increase of about 25% of the OOP strength of a four-borders constrained panel than another with three borders restricted, even if the cracking pattern was similar. Nonetheless, the authors highlighted that those two specimens showed some OOP displacement capacity, while a wall with two borders constrained (top and bottom interfaces) experienced a brittle failure due to masonry crushing soon after reaching the maximum strength. Earlier, Angel, et al. [20] concluded that infill-frame boundary conditions were affected by the previous IP loading demands. Tu et al. [29] found in their experimental study that the OOP strength capacity can be improved if the infill wall boundaries are properly strengthened, preventing the fragile OOP detachment. Careful reflection must be conducted on this issue concerning the type of masonry unit used (i.e. solid bricks, horizontal hollow bricks or vertical hollow bricks). Hollow bricks are more fragile, particularly clay units, meaning that sometimes the crushing of the bricks for low OOP seismic demands can avoid the arching mechanism development.

The available data from the tests of masonry infill walls subjected to pure OOP loads is not enough, considering the several parameters that affect its performance. Also, most of these studies only discuss the OOP behaviour response in terms of damage evolution, force-displacement curves, maximum strength and deformation capacity of the walls. However, no studies evaluated in detail the damage evolution or the viscous damping in the case of OOP cyclic loading. In addition, a large percentage of those tests is monotonic, which means that the study of energy dissipation, viscous damping and damage evolution due to cyclic loading cannot be addressed. It is fundamental to increase the knowledge concerning their non-linear behaviour when subjected to cyclic loadings.

Concerning the definition of damage limit states for masonry infill walls under OOP loadings, only the study carried out by Cardone and Perrone [30] slightly introduced this issue. The authors developed fragility curves and loss functions for masonry infill walls subjected to seismic actions. The authors proposed damage states for each fragility curve to characterize the damage development. The authors did not provide significant details concerning the methodology that supported the damage states. However, they are related to walls subjected to only combined in-plane and out-of-plane seismic loadings. They do not specify the damage evolution due to the OOP loading demands. Nevertheless, it should be mentioned that only one specific damage is attributed to the OOP effect within the four damage states. Namely, the fourth damage state only points out the possible occurrence of the out-of-plane collapse.

Also, other numerical investigations were developed to provide drift limits for characterizing the IP-OOP interaction. Namely, the authors proposed experimentally calibrated interaction IP/OOP interaction domains to identify the limit states of thin masonry panels, with and without strengthening solutions [22,31].

Based on this motivation, the primary purpose of this manuscript was to propose damage states for masonry infill walls subjected to OOP loadings. After that, a pilot damage index is proposed for masonry infill walls made of hollow clay horizontal brick units. The third objective of this work was the assessment and discussion of their normalized energy dissipation capacity and their hysteretic viscous damping. Some analytical formulations were proposed to estimate these parameters using an empirical-based approach. A database containing thirteen OOP tests performed in three different research works was used to achieve these goals.

2. Database overview

2.1. Specimens description

The database used for this research work comprises a total of 13 masonry infill walls that were subjected to OOP tests, using a distributed loading approach (i.e. airbags or pneumatic actuators), and were subjected to a charge-discharge (half-cyclic) loading sequence. The database is subdivided into four groups, namely: Group 1 - four tests carried out by Furtado et al. [32]; Group 2 – four specimens tested by Furtado et al. [33] and one test carried out by De Risi et al. [25]; Group 3 – one test carried out by Agante et al. [34]; Group 4 – three tests carried out by Akhoundi et al. [35].

The division into four groups was based on the following criteria: i) OOP load application approach (Group 1 and 2); ii) type of masonry unit (Group 3); and iii) specimens scale (Group 4). Groups 1 and 2 are comprised of masonry infill walls made of hollow clay horizontal brick units and were divided according to the OOP load application approach. Thus specimens Inf_02, Inf_04 Inf_05 and Inf_06 belong to Group 1 (OOP loading is applied with airbags) and specimens Inf_08, Inf_09 Inf_15 and Inf_16 belong to Group 2 (OOP loading is applied with pneumatic actuators).

The specimen LWC_OOP was included in Group 3 since it is a lightweight concrete block wall with an OOP response different from the walls made of hollow clay bricks. Finally, group 4 is comprised of scaled specimens made of hollow clay brick units. The specimens SIF–O-1L-A, SIF–O-1L-B and PIF-O-1L-B, were not included in Group 1 to assess any possible scale effect.

Table 1 presents a summary of information concerning the specimens selected for this research study. Nomenclature of the specimens, geometric dimensions, type of OOP loading application, masonry unit and possible variables under investigation are presented. Please note that the loading shape applied by the airbags is parabolic with high amplitude at the panel mid-height. On the other hand, the loading shape applied by the pneumatic actuators is purely uniform along the entire wall height.

The monotonic OOP tests and the OOP tests of infill walls with prior IP damage available in the literature were excluded from this study since the focus of this study are the pure OOP cyclic or semi-cyclic tests. The review study carried out by Anić et al. [7] showed that a large part of the OOP tests of masonry infill walls was performed by applying a monotonic load based on different approaches (one-point, four-points, eight-points).

Table 1
Summary of the database specimens.

Group	Specimen	Wall geometric dimensions (mm) Length x Height	OOP loading application	Masonry unit	Plaster	Openings	Axial load ratio on each column	Panel support conditions	Workmanship[d]
1	Inf_02	4200 × 2300	Airbags	HCHB[b] 150 mm	No	No	No	Full	No
	Inf_04				No	No	0.16 (axial load: 270 kN)	Full	No
	Inf_05				No	No	No	2/3 thickness supported[e]	No
	Inf_06				10 mm	No	No	Full	No
2	Inf_08	4200 × 2300	Pneumatic atuators	HCHB 150 mm	10 mm	No	No	Full	No
	Inf_09				10 mm	No	No	Full	Yes
	Inf_15				10 mm	Window (15%[f])	No	Full	No
	Inf_16				10 mm	Door (22%[f])	No	Full	No
	AB-OOP			HCHB 110 mm	No	No	No	Full	No
3	LWC_OOP	4200 × 2300	Pneumatic actuators	LWCB[c] 315 mm	No	No	No	Full	No
4	SIF–O-1L-A	2415 × 1635[a]	Airbags	HCHB 80 mm	No	No	0.40 (axial load: 160 kN)	Full	Yes
	SIF–O-1L-B				No	No	0.40 (axial load: 160 kN)	Full	No
	PIF-O-1L-B				No	Window (12.8%)	0.40 (axial load: 160 kN)	Full	No

[a] Specimens are 1/2 Scaled.
[b] Hollow Clay Horizontal Brick.
[c] Light Weight Concrete Block.
[d] Masonry wall constructed using different operators.
[e] Masonry wall partially supported in the bottom beam.
[f] Percentage of the opening area relative to the panel area.

2.1.1. Group 1

Furtado et al. [32] studied the effect of plaster (Inf_06), panel support conditions (Inf_05) and axial load (Inf_04) applied on the adjacent columns on the OOP behaviour of full-scale masonry infill walls. The walls' geometric dimensions were 4.20 × 2.30 m^2 (length x height), as shown in Fig. 1a. Hollow clay horizontal brick units 150 mm thick were used. The envelope frame was composed of columns and beams with cross-sections of 0.30 × 0.30 m and 0.30 × 0.50 m, respectively. The columns longitudinal reinforcement are 4ø16+2ø12 and a transversal reinforcement of ø8//0.05 m along with the plastic regions and ø8//0.15 m in the remaining column extension. On the other hand, the longitudinal reinforcement of the beams is 5ø16 with a transverse reinforcement of ø8//0.10 m in their plastic hinge regions and ø8//0.20 m in their middle-length.

Specimen Inf_02 was the reference test since it was built without plaster, fully supported in the bottom RC beam and without axial load on the adjacent RC columns. The specimen Inf_04 was constructed with the same geometric and material characteristics as the reference specimen Inf_02. In each column, an axial load of 270 kN (axial load ratio equal to 0.16) was applied to simulate the dead loads' effect. It will be possible to assess its impact on the OOP response of the masonry infill walls in subsection 2.5.1.

Based on this justification, an axial load of 270 kN (axial load ratio of 0.16) was applied in each column to simulate the expected dead load.

Inf_05 was constructed with the same characteristics and tested without axial load on the columns. The difference was that the wall was built with 2/3 of its thickness supported in the bottom beam. Finally, the specimen Inf_06 was constructed with 1 cm plaster. All the walls were built without reinforcement and openings. More details concerning the material and mechanical properties can be found in Ref. [32] and in subsection 2.3. The OOP loading was applied using airbags. More information related to the test setup will be provided in 2.4.

The specimens from Group 1 were constructed using the same workmanship and the same construction methodology. No mechanical connection was included in the panel-frame boundaries. The connection between the upper beam and the panel, which determines a three or four-sided constraint, is performed by applying the mortar.

2.1.2. Group 2

Group 2 is comprised of five specimens, four tested by Furtado et al. [33] and one tested by De Risi et al. [25]. Furtado et al. [33] tested four full-scale masonry infill walls with 4.20 m length and 2.30 m height, as shown in Fig. 1a. The walls were built using the hollow clay horizontal bricks 150 mm thick and 10 mm plaster. The reference specimen in Group 2 was the wall Inf_08.

Specimens Inf_08 and Inf_09 were built with different qualified operators but using the same construction methodology and materials. Besides the recommendation of adopting the same construction methodology, the workmanship parameter is an uncontrolled one since it depends from operator to operator. The thickness of the mortar bed joints, arrangement of bricks, preparation of mortar was supervised by the authors of this manuscript. The workmanship effect was studied with these two specimens.

Moreover, the authors investigated the effect of the opening with the specimens Inf_15 and Inf_16. Specimen Inf_15 is a wall with a central window with the geometric dimensions of 1.25 × 1.15 m^2 (opening area ratio is 15%.), length and height, respectively, as shown in Fig. 1b. Finally, Inf_16 was an infill wall with a central door with the geometric dimensions of 1.25 × 1.70 m^2, respectively, length and height, as shown in Fig. 1c. The opening area ratio is 22%. The dimensions and detailing of the surrounding RC frame are

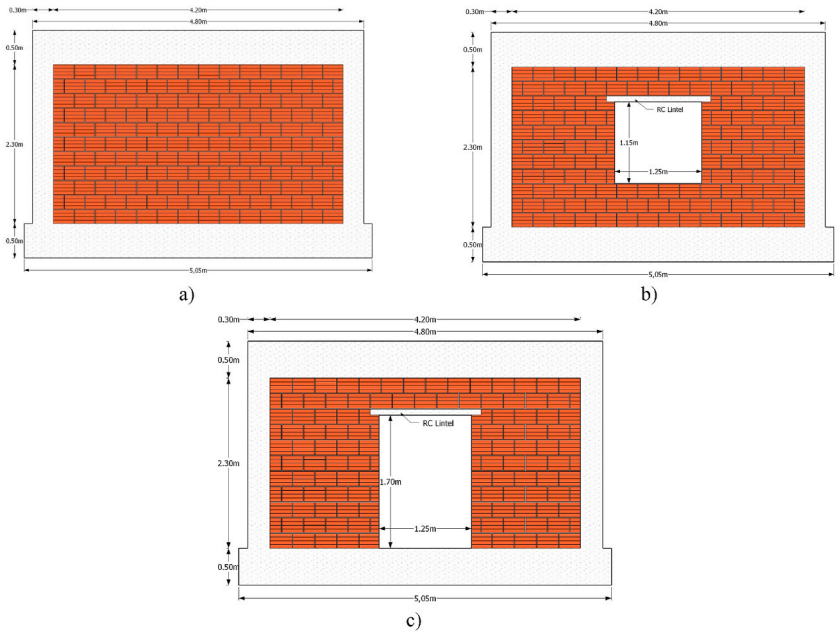

Fig. 1. Specimens geometry: a) Inf_02, Inf_04, Inf_05, Inf_06, Inf_08, Inf_09, LWC_OOP and AB-OOP; b) Inf_15 and; c) Inf_16.

Table 2
Summary of the material properties.

Group	Specimen	Masonry unit compressive strength[a] (Mpa)	Plaster compressive strength (Mpa)	Plaster Flexural strength (Mpa)	Masonry walls compressive strength (Mpa)	Elastic Modulus (Mpa)	Masonry walls diagonal tensile strength (Mpa)	Shear Modulus (Mpa)	Masonry walls parallel flexural strength[b] (Mpa)	Masonry walls perpendicular flexural strength[c] (Mpa)
1	Inf_02	1.04 CoV = 23.6%	12.6[e]	5.7[e]	1.09 CoV = 12.8%	1975 CoV = 36.7%	0.65 CoV = 22.2%	996 CoV = 8.9%	0.22 CoV = 17.6%	0.30 CoV = 7.9%
	Inf_04		11.9[e]	4.5[e]						
	Inf_05		4.45[e]	1.79[e]						
	Inf_06		7.75[e]	2.47[e]						
2	Inf_08		5.24[e]	1.90[e]						
	Inf_09		4.49[e]	1.72[e]						
	Inf_15		4.22[e]	1.66[e]						
	Inf_16		4.09[e]	1.46[e]						
	AB-OOP	1.08 CoV = 19.7%	4.75[e]	2.12[e]	N/R	N/R	N/R	N/R	N/R	N/R
3	LWC_OOP	2.10[f] CoV = 9.88%	6.58[e]	2.43[e]	2.60 CoV = 13.2%	2424 CoV = 24.3%	0.20 CoV = 5.7%	1389 CoV = 36.1%	0.08 CoV = 14.2%	0.17 CoV = 25.2%
4	SIF–O-1L-A	1.57 CoV = 15.1%	2.76 to 6.18 CoV = 5% and 5.8%[d]	1.20 to 2.51 CoV = 9% and 6%[d]	1.17 CoV = 4.8%	1155 CoV = 29.8%	0.24 CoV = 9%	1252.8 CoV = 1.1%	0.053 CoV = 6.4%	0.29 CoV = 14%
	SIF–O-1L-B									
	PIF-O-1L-B									

[a] Compressive strength perpendicular to the horizontal holes.
[b] Flexural strength parallel to the horizontal bed-joints.
[c] Flexural strength perpendicular to the horizontal bed-joints.
[d] The authors do not provide the specific value for each masonry wall's plaster compressive and flexural strength. The authors only provide the average range results.
[e] The authors do not provide the Coefficient of Variation (CoV).
[f] Results obtained from compressive strength tests parallel to the vertical holes.

the same as the one used by Furtado et al. [32]. No gap or reinforcement was used between the wall and the frame. In both specimens, an RC lintel was built at the top of the opening with 1.65 m length and 0.10 m height. The longitudinal reinforcement used in the lintel was 3ø6mm diameter.

The summary of the material properties of these specimens can be found in sub-section 2.3. More detailed information concerning the material and mechanical properties can be found in Ref. [33]. The specimens of Group 2 were subjected to distributed OOP loads applied by pneumatic actuators. More details concerning the test setup will be provided in 2.4.

The fifth specimen that comprised this Group 2 was tested by De Risi et al. [25]. The wall is made of hollow clay horizontal brick units 110 mm thick. The authors used the same wall geometry, RC frame dimensions and detailing and test setup used by Furtado et al. [33]. No gap or reinforcement was used between the wall and the frame. Sub-section 2.3 presents a summary of the material properties of these specimens, but more details concerning these specimens can be found in Ref. [25].

2.1.3. Group 3

Group 3 consisted of one specimen tested with a different masonry unit used to construct the wall. The test belongs to the testing campaign carried out by Agante et al. [34]. The authors tested an infill wall made of lightweight concrete blocks with improved thermal energy and acoustic properties. The authors used the same wall geometry, RC frame dimensions and detailing and test setup used by Furtado et al. [33]. Again, no gap or reinforcement was used between the wall and the frame. More details concerning the material and mechanical properties can be found in sub-section 2.3 and in Ref. [34].

2.1.4. Group 4

Group 4 comprises three tests carried out by Akhoundi et al. [35] to study the effect of the workmanship and of openings. The three specimens were half-scaled with respect to the geometry of the specimens tested by Furtado et al. [32]. The length of the walls was 2415 mm and the height 1635 mm. The RC frame was designed with columns with a cross-section of 160 × 160mm^2, with a reinforcement detailing comprised of 4ø8mm+2ø6mm with a transverse reinforcement of ø4//70 mm. The cross-section adopted for the top and bottom beams was 270 × 160mm, with 2ø10mm+3ø8mm (top reinforcement) and 2ø6mm (bottom reinforcement) in their plastic hinges extension (0.50 m). Regarding the beams' longitudinal reinforcement in the middle-span is 2ø6mm (top reinforcement) and 3ø10mm+2ø6mm (bottom reinforcement). The transverse reinforcement was ø4//120 mm.

The reference specimen was the wall SIF–O-1L-B, built by labor type B and without openings. The second specimen, SIF–O-1L-A, was built by labour type A and without openings, to assess the workmanship effect in the OOP behaviour. Finally, specimen PIF-O-1L-B consisted of a wall with a central window with an opening ratio equal to 12.8% and was built by labour type B. The masonry units selected to construct these specimens were hollow clay horizontal bricks 80 mm thick. No gap or reinforcement was used between the wall and the frame. More details concerning the material and mechanical properties can be found in sub-section 2.3 and in Ref. [35].

2.2. Material properties

The compilation of the material and mechanical properties of the thirteen masonry infill walls under study are herein presented and discussed. Compressive strength tests perpendicular to the holes were performed on several brick units according to the standard EN 772–1 [36]. Compressive and flexural strength tests were done on mortar samples collected during the wall's construction. Concerning the masonry infill walls properties, compressive strength tests were performed according to EN 1052–1 [37]. Also, diagonal tensile strength tests were performed according to RILEM TC-76-LUM [38], from which it was determined the diagonal tensile strength and shear strength. Finally, flexural strength tests were conducted according to EN 1052–2 [39]. Table 2 summarizes the average results and coefficient of variation (CoV) obtained in each test.

Concerning the compressive strength of the masonry units, the LWC blocks achieved the highest result with an average value of 2.10 MPa, about 2.2 times higher than the hollow clay horizontal bricks 150 mm thick used in Group 1 and 2, which is the lowest one. Regarding the plaster properties, it can be seen that apart from specimens Inf_02 and Inf_03, the average compressive strength ranges between 4.09 and 6.58 MPa, and the flexural strength varies between 1.27 and 2.51 MPa. These results are in agreement with an M5 class mortar. The mortar results from the walls Inf_02 and Inf_03 are slightly higher than the remaining ones, but the authors do not justify that. The compressive strength tests on masonry infill walls specimens show that the ones made of LWC blocks reached the highest result with an average value of 2.60 MPa. Once again, the walls made of the hollow clay horizontal bricks 150 mm obtained the lowest mark (1.09 MPa), about 59% lower than those used in Group 3. The highest and lowest elastic modulus were obtained by the walls of Group 3 and 4, respectively.

On the contrary, the highest tensile strength was achieved by Group 1, about 3.25 times higher than Group 3 (lowest value). Finally, the flexural strength tests carried out in both directions (i.e. parallel and perpendicular to the horizontal bed joints revealed that the walls from Group 1 always reached the highest result and Group 3 the lowest one.

2.3. Description of the test setup

2.3.1. Group 1

The OOP tests performed in group 1 consisted of applying a distributed OOP load through nylon airbags. A self-equilibrated reaction steel structure was attached to the RC frame in twelve different points, and the airbags were placed between the panel and the reaction structure. The steel reaction structure is composed of five vertical steel I-shape profiles and four tube profiles. A wood plate with 10 mm thickness was placed in the front of the steel structure to support the airbags. In this group, the wall Inf_04 was tested with axial load applied on the adjacent columns.

The axial load was applied by means of a hydraulic jack inserted between a steel cap placed on the top of each column and an upper

steel profile, which, in turn, was connected to the foundation steel shape resorting to a pair of high-strength rods per column. Hinged connections were adopted between these rods and the top and foundation steel shapes. The axial load applied to the columns was continuously measured by load cells inserted between the jacks and the top of each column. Fig. 2a shows a general view of the test setup used in Group 1.

Concerning the OOP tests protocol, two half-cyclic OOP displacements were imposed with steadily increasing displacement levels, targeting the following nominal peak displacements: 0.5, 1; 1.5; 2; 2.5; 3.5; 5; 7.5; 10; 15; 20; 25; 30; 35; 40; 45; 50; 50; 55; 60; 65, 70, 75, 80, 85, 90, 95 and 100 mm.

The central geometric point of the infill wall was selected as the reference point since it was expected that is the region where it will occur the largest deformation of the panel, as adopted by other authors [40,41]. The OOP drift values corresponding to those target

Front view

Back view

a)

Front view

Back View

b)

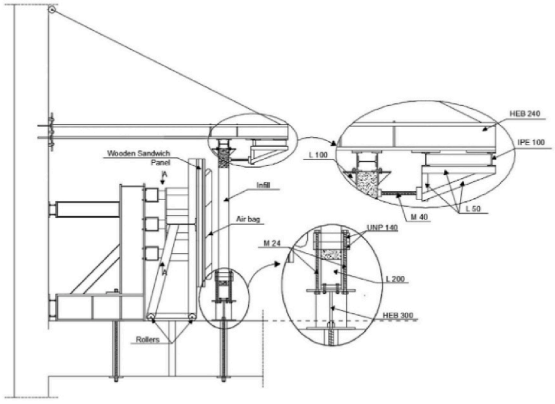

Lateral view

c)

Fig. 2. Test setup general view: a) Group 1; b) Group 2 and 3 and; c) Group 4.

displacement levels (computed according to the wall reference point) are: 0.043%, 0.087%; 0.13%; 0.17%; 0.22%; 0.30%; 0.43%; 0.65%; 0.87%; 1.30%; 1.74%; 2.17%; 2.61%; 3.04%; 3.48%; 3.91%; 4.35%; 4.78%; 5.22%; 5.65%; 6.09%; 6.52%; 6.96%; 7.39%; 7.83%; 8.26% and 8.70%.

Concerning the wall Inf_04, the axial load of 270 kN was applied in each column before beginning the OOP test. More details regarding this test setup can be found in Ref. [16].

2.3.2. Groups 2 and 3

The test setup used to perform the OOP tests of specimens from Group 2 and 3 is similar to the one presented in 2.3.1. Again, the distributed OOP loading was applied through several pneumatic actuators that mobilized the entire infill panel surface with wood plates (one per actuator) placed between the actuators and the panel. All the pneumatic actuators are linked to four horizontal alignments, which react against five vertical alignments. The horizontal alignments are coupled with hinged devices that allow lateral sliding. The steel reaction structure was also attached to the RC frame in the same twelve points used in the test setup from group 1, with steel bars coupled with load cells to monitor the OOP loadings. This self-equilibrated system balances the transmission of the OOP loadings to the reaction frame. The test setup configuration used to test Inf_08, Inf_09, LWC_OOP and AB_OOP can be found in Refs. [15,25,32]. Fig. 2b shows a general view of the test setup used in Group 2 and 3.

The disposition of the pneumatic actuators was re-arranged to test the walls with the openings. For this, some pneumatic actuators were removed in the opening region. This test setup allowed the authors to perform the OOP tests until the wall collapse without damaging any equipment. The testing protocol followed the same steps described in section 2.3.1. The reference point was the same used in 2.3.1. No axial load was applied at the top of the adjacent RC columns in the tests of this group. More details regarding this test setup can be found in Ref. [16].

2.3.3. Group 4

The out-of-plane loading was applied using an airbag installed between the infill wall and a stiff wooden sandwich panel attached to a reaction steel structure. This structure was connected to the lateral reaction wall and the reaction floor to prevent uplifting and sliding during the test. The steel structure was stiffened at the top with a horizontal steel profile and with inclined steel profile. The wooden sandwich panel was connected to the steel structure using four load cells to measure the OOP loads applied by the airbag to the brick infill wall. The OOP displacement at the top RC beam was restrained by attaching steel profiles at each side of the upper concrete beam, bolted to the top steel frame. Fig. 2c shows a general view of the test setup used in Group 4.

The three specimens were tested with a prior application of an axial load of 160 kN on each column by hydraulic actuators linked to the horizontal foundation steel profile through high prestressed bars. The OOP tests were performed under displacement control. The central geometric point of the wall was selected as a reference point to control the loading application. Two half-cyclic OOP displacements were imposed with steadily increasing displacement levels, targeting the following nominal peak displacements: 0.5; 1; 1.5; 2; 2.5; 3.5; 5; 7.5; 10; 15; 20; 25; 30; 35; 42; 50 and 80 mm. The OOP drift values corresponding to those target displacement levels (computed according to the wall reference point) are: 0.08%, 0.16%; 0.24%; 0.32%; 0.40%; 0.56%; 0.80%; 1.20%; 1.61%; 2.41%; 3.22%; 4.02%; 4.82%; 5.63%; 6.75%; 8.04% and 9.65%.

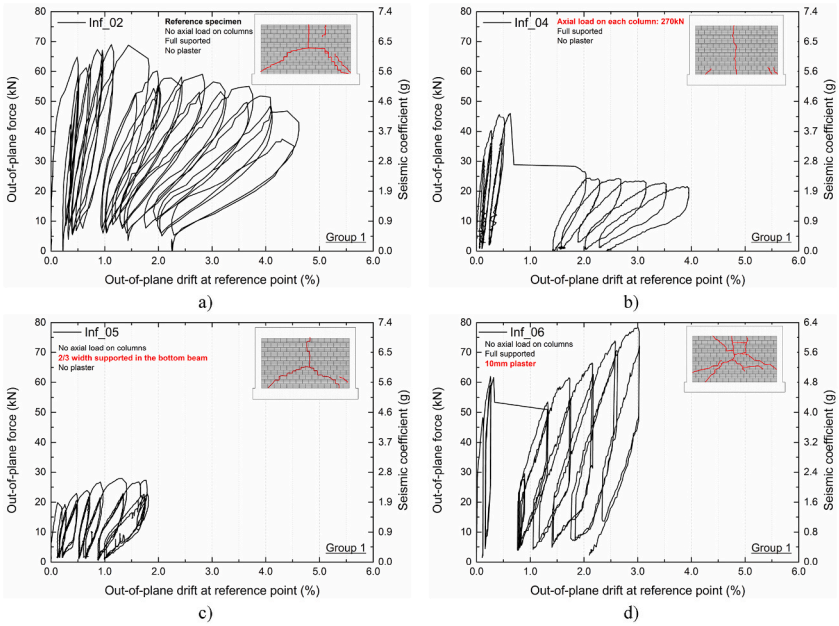

Fig. 3. Group 1: OOP Force vs drift response curves and seismic coefficient a) Inf_02 (reference specimen); b) Inf_04; c) Inf_05 and d) Inf_06.

2.4. Summary of the test results

2.4.1. Group 1

From the analysis of the Group 1 OOP force-drift curves, plotted in Fig. 3, it can be stated that the reduction of the panel width support (2/3 of the panel thickness) was the parameter that reduced more the wall strength. The reference specimen Inf_02 reached a maximum strength of 67.04 kN and presented a trilinear cracking pattern, as shown in Fig. 3a. It can be noticed that the reduction of the panel support width to 2/3 of its thickness, specimen Inf_05, reduced the OOP maximum strength by about 59%, as shown in Fig. 3c. However, both walls presented the same trilinear cracking pattern, typical of a panel with three borders constrained and one not fully restrained. The axial load application on the top of each RC column, specimen Inf_04, reduced the wall strength by 31% and modified the cracking pattern. Instead of the trilinear cracking, the wall Inf_04 presented a vertical linear cracking, typically of a panel under one-direction flexure, as presented in Fig. 3b. The plaster increased the wall strength by about 16% and caused the cracking spread, as shown in Fig. 3d by wall Inf_06. However, the authors reported that some cracks could only be related to the plaster cracking and not to the masonry crack.

The seismic coefficient was calculated by dividing the out-of-plane force by the mass of the panel. The OOP drift at the reference point was computed by considering half of the panel height since the largest displacements were observed at the panel mid-height.

2.4.2. Group 2

In Group 2, the parameters under study were the workmanship (Inf_09), and the openings (Inf_15 – window and Inf_16 - Door). The reference wall Inf_08 presented a trilinear crack and reached a maximum peak load of 44.22 kN, as shown in Fig. 4a. The use of different labour slightly modified the wall cracking pattern, as observed in Fig. 4b. Surprisingly, specimen Inf_09 presented an OOP strength 39% higher, proving that the uncertainty associated with the workmanship is still worth investigating the masonry infill walls seismic behaviour nowadays.

Regarding the effect of the opening, it was observed in the wall with a central window (Inf_15) the development of cracks from the opening corners towards the wall corners. Small additional cracks were reported. The maximum OOP strength reached by the wall was 27% lower than the one achieved by the reference Inf_08, as shown in Fig. 4c. However, the corresponding seismic coefficient was only 15% lower due to the opening. The wall Inf_15 presented a higher deformation capacity than the reference specimen about 2.5 times.

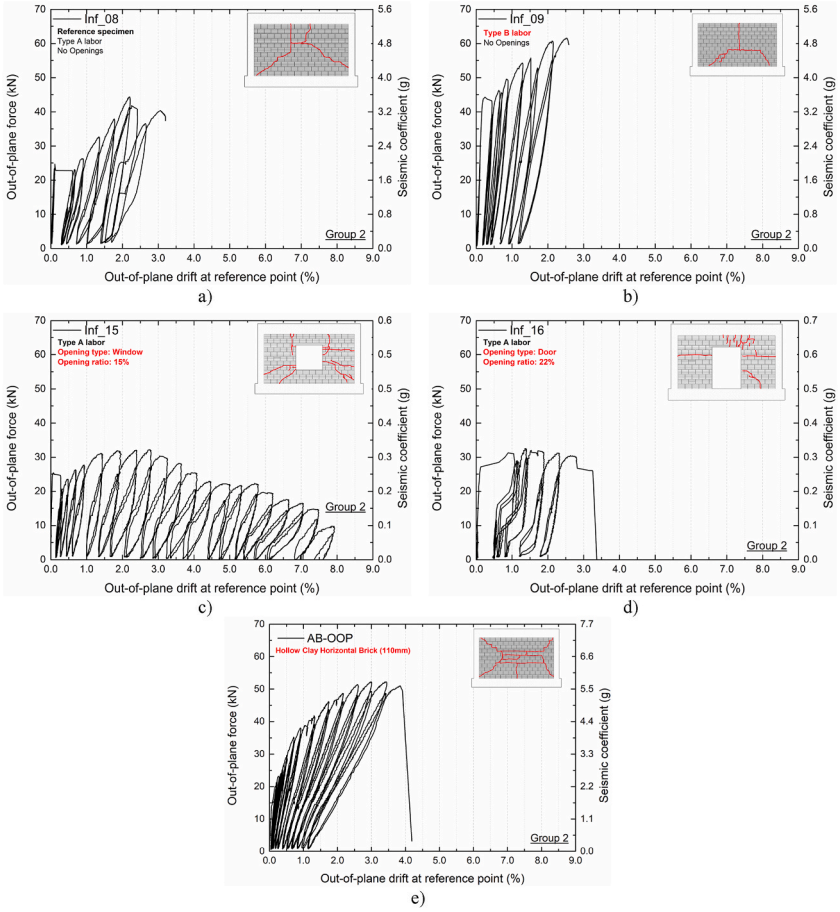

Fig. 4. Group 2: OOP Force vs drift response curves and seismic coefficient a) Inf_08 (reference specimen); b) Inf_09; c) Inf_15, d) Inf_16 and e) AB-OOP.

Moreover, the wall with a central door (Inf_16) presented a central horizontal crack located near the top of the opening. Other ones were observed on the wall right side and some others at the top of the opening. The maximum strength was 26% lower than the reference specimen, as shown in Fig. 4d. However, the seismic coefficient was only 6% lower than the reference specimen.

Finally, it can be observed from the force-displacement curve of wall AB-OOP, shown in Fig. 4e, that it reached an OOP strength that increased progressively up to 52.5 kN without any strength drop.

2.4.3. Group 3

The main aim of the group 3 test was to assess the effect of using a different masonry unit type. The result is herein presented in Fig. 5. The wall LWC_OOP obtained a high OOP strength equal to 229.6 kN. In addition, the wall presented a trilinear cracking and other additional diagonal cracks, which resulted from the arching mechanism.

2.4.4. Group 4

The two variables assessed in group 4 tests were the workmanship and the openings. The reference specimen SIF–O-1L-B presented a 5-linear cracking and a maximum strength of about 39.8 kN, as shown in Fig. 6a.

The wall SIF–O-1L-A was built with different labour and it was found that the cracking pattern changed to a trilinear cracking, and the OOP maximum strength reduced about 13.3% (see Fig. 6b). Finally, the existence of a central window (Fig. 6c) did not affect the OOP strength, with a slight reduction of only 1.5%. Nonetheless, the seismic coefficient was 12% higher than the one of the wall SIF–O-1L-B. The cracking pattern was characterized by diagonal cracks from the opening corners towards the wall corners.

2.4.5. Global analysis

The summary of the results from the thirteen OOP tests is presented in Table 3. The maximum OOP strength, seismic coefficient and cracking pattern obtained by each specimen are described in the Table. Different observations can be drawn comparing the OOP maximum strength results and the seismic coefficients. It becomes clear that the maximum one was always reached by the specimen LWC_OOP in both response parameters due to the type of masonry unit (2 times larger than HCHB 150 mm and 3 times larger than HCHB 100 mm). However, the difference in terms of the seismic coefficient is considerably lower. For example, the maximum OOP strength of the wall LWC-OOP is 2.94 times higher than Inf_06.

On the other hand, the seismic coefficient is only 1.31 times higher. The mass of the wall LWC-OOP (2.23 times higher) justifies this difference. Again, in both response parameters, the lowest result was Inf_05 due to the reduction of the panel support width that reduces the strength provided by the arching mechanism.

Concerning the OOP maximum strength, it is possible to observe that the specimens from Group 4 reached, on average, lower results ranging between 34 and 40 kN. However, the same was not observed in the seismic coefficient since the mass balanced this response parameter. Thus, the seismic coefficient varies in group 4 between 5.61 g and 7.18 g, higher than Group 1 (2.58–6.27 g) and Group 2 (3.04–4.94 g). The difference found in the seismic coefficient is directly related to the lower value of the Group 4 walls mass.

Furthermore, it can be noticed that the openings did not reduce the seismic coefficient since, in Group 2 and Group 4, the walls with openings exceeded the result obtained by the reference specimen. The opening only reduced the deformation capacity of specimen PIF-O-1L-B in opposite to what was observed in the remaining Group 2 walls. The authors believe that these contradictory results need future investigations (experimental and numerical) to justify the variations in deformation and/or strength capacity. Using a lintel at the top of the opening may have contributed to the wall initial stiffness and strength. Detailed numerical models would also help to clarify the lintel effect in walls with different types of openings.

Pradhan et al. [42] reviewed the experimental studies on the OOP behaviour of infill walls to analyze the influencing parameters. The authors concluded that the available results have shown that small openings like doors and windows do not highly influence OOP strength. They stressed that more tests are necessary to better understand how openings affect the OOP capacity of the infill wall.

As previously mentioned, the wall AB-OOP was included in Group 2 since it is a wall made of hollow clay horizontal brick units and was subjected to an OOP load using pneumatic actuators. The differences between this specimen and the others from group 2 (Inf_08,

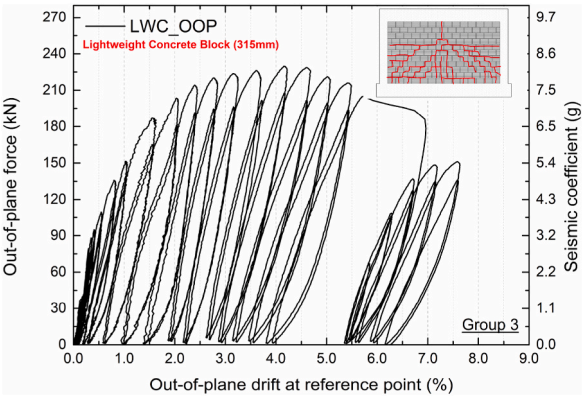

Fig. 5. Group 3: OOP Force vs drift response curves and seismic coefficient: LWC_OOP.

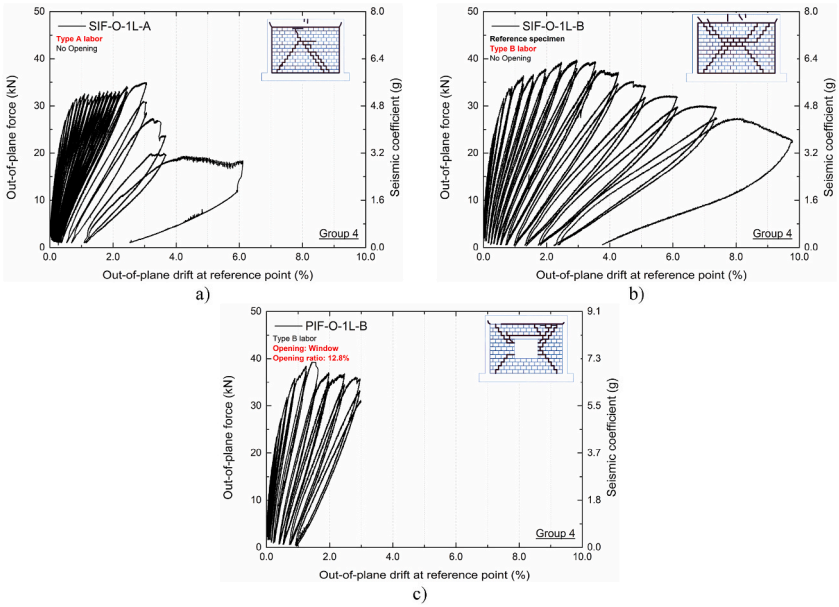

Fig. 6. Group 4: OOP Force vs drift response curves and seismic coefficient a) SIF–O-1L-A; b) SIF–O-1L-B, and c) PIF-O-1L-B [35].

Table 3
Summary of the test results.

Specimen	Fmax (kN)	Seismic Coefficient (g)	Cracking pattern/failure mode
Inf_02	67.04	6.21	3-linear cracking
Inf_04	45.98	4.26	1-vertical cracking
Inf_05	27.82	2.58	3-linear cracking
Inf_06	78.15	6.27	3-linear cracking
Inf_08	44.2	3.55	3-linear cracking
Inf_09	61.49	4.94	3-linear cracking
Inf_15	32.2	3.04	Diagonal cracks from the openings to the panel corners
Inf_16	32.48	3.34	Diagonal cracks from the openings to the panel corners
LWC_OOP	229.6	8.24	3-linear cracking
AB-OOP	52.5	5.75	5-linear cracking
SIF–O-1L-A	34.94	5.61	3-linear cracking
SIF–O-1L-B	39.8	6.39	5-linear cracking
PIF-O-1L-B	39.25	7.18	Diagonal cracks from the openings to the panel corners

Inf_09) are i) thickness of the masonry units (110 mm in the case of AB-OOP and 150 mm in the others) and ii) plaster (without plaster – AB-OOP and with plaster – others). The arching mechanism appears to be activated more in this panel than in the other thicker infills, contributing to the wall OOP strength. More complementary tests must be performed to clarify the slenderness ratio effect (i.e. height/thickness) on the cracking and strength of the wall under pure OOP loadings.

Finally, most of the walls without openings presented a trilinear cracking (7 out of 10), and the ones who not showed this pattern were limited by the axial load applied on the columns (Inf_04), the use of a thin masonry unit and the different workmanship (AB-OOP and SI–O-1L-A). It is not clear the reason behind this cracking pattern modification. Potential reasons that can justify this modification are: i) experimental variability; and ii) difficulties in filling the top frame-wall interface with mortar, which can create uncertainty related to the characteristics of the top boundary of the wall.

The walls with windows presented a cracking pattern similar to each others, characterized by the diagonal cracks from the opening corners to the wall corners. It should be remarked that the wall Inf_15 was constructed with an RC lintel and the specimen PIF-O-1L-B was not. Nevertheless, this detail did not modify and create any variation of the cracking pattern. Regarding the wall with a central door (Inf_16), there was a different behaviour on its left and right sides. Again, an RC lintel was constructed at the top of the opening. Due to the configuration of the cracking pattern, it becomes evident that the RC lintel could have contributed to this behaviour. Unfortunately, one test is not sufficient to draw a solid conclusion on this issue. Future investigations need to be carried out combining walls with different opening percentages with and without RC lintel.

3. Damage evolution in masonry infill walls under OOP loading

When subjected to OOP loading demands, the damage development in masonry infill walls directly causes the gradual stiffness and

strength degradation. The damage observed in panels only subjected to OOP loading demands cannot be compared to those observed in walls subjected to combined IP-OOP loadings, since the IP seismic loadings can introduce damage scenarios that increase their OOP vulnerability. As previously remarked, the number of experimental tests available in the literature to study the OOP seismic behaviour of infill walls is still insufficient, considering the several parameters and variables that can affect their response [7].

It is known that the cracking pattern is directly related to the boundary conditions of the wall. Di Domenico et al. [43] carried out a testing campaign comprising three specimens with different boundary conditions. One wall was mortared along all four edges of the wall, and a wall provided a gap equal to 2 mm between the upper edge and the top beam. Finally, the third specimen was restrained to the confining frame only along the upper and lower edges. From the tests, the authors observed that two-way arching was activated for the wall four boundaries constrained, being visible a five linear cracking. A vertical hairline crack was observed in the wall with three edges constrained (i.e. wall with a gap between the wall and top beam). This observation is consistent with the expected cracking pattern for this type of wall in which only horizontal arching can occur reported in Ref. [27]. In the wall with only two edges constrained (upper and lower), a one-way arching way was observed with a pure horizontal crack at the middle height of the wall.

The following sub-sections will provide a detailed discussion on the different damage states experienced by the masonry infill walls during the purely OOP tests. In addition, the relationship between the damages and the corresponding OOP drift demand is also reported.

3.1. Definition of damage states

The test was stopped at the end of each target displacement for each specimen to observe and record the damage evolution. This procedure allowed registering the development of new cracks and the expansion of the existing ones. Group 4 was excluded from this analysis since the authors did not provide information concerning the damage evolution. Based on those observations, the damage observed can be grouped into four different damage states, namely: First cracking (damage state 1); Moderate damage (damage state 2); Extensive damage (damage state 3); and Collapse (damage state 4). Table 4 summarizes the damage states herein proposed for the masonry infill walls subjected to OOP loadings, based on the observation of the typical evolution of damage under increasing OOP displacement demand.

Several examples of damages observed for each damage state are presented along this sub-section. For each damage state, the damages observed in the walls of only one of the groups under study are shown to ensure that the walls were subjected to the same OOP loading approach, excluding any possible effect. However, it needs to be reinforced that the examples presented for each damage state are representative of those that occurred in the specimens from the other groups. To avoid the repetition of those images, the authors did not include the damages observed in all the walls for all the damage states.

3.1.1. Damage state 1

It was possible to watch that the first crack varied in length and pattern from test to test from observing the tests. The first crack observed in specimens from Group 1 is presented in Fig. 7. It is possible to observe different cracking shapes: vertical ones (short and long length) and diagonal ones. In the remaining groups, the development of a first horizontal crack located at the panel mid-span and mid-height was observed most of the time. Even in the panels with openings (Inf_15 and Inf_16), a first horizontal crack was reported to be located at mid-span and mid-height next to the opening. The loading application type can justify the modification of the cracking direction since in group 1 the load was applied through airbags. The airbags OOP load shape reproduces the deformed shape itself, as can reported by other authors [44,45]. In other words, the load distribution is shaped as a parabolic shape with high strength capacity at the middle height of the wall and less strength near the boundary limits. In the remaining walls, pneumatic actuators were used to apply the OOP force. The shape of the OOP load is uniform along the entire panel height and length. Looking at the results of Inf_15 and Inf_09, the length of these cracks varied from 0.30 m to 3 m, respectively.

Further studies need to be performed to clarify the impact of the OOP load application in the response of the wall. As mentioned

Table 4
Proposal of damage states and the corresponding description.

	Damage state	Description of the damages observed
Repairability limit	First Cracking (Damage state 1)	- corresponds to the first visible crack, which usually corresponds to the reduction of the panel stiffness (other authors considered the development of the first cracking as the first damage state of an infill wall under pure OOP loads [40])
	Moderate Damage (Damage state 2)	- extension of the first crack observed in damage state 1 - development of cracks with a corresponding extension higher than 30 cm with thickness not larger than 1 mm - slight plaster detachment in the wall-frame interfaces - slight OOP detachment of the wall from the surrounding frame
	Extensive Damage (Damage state 3)	- The cracking pattern of the wall is evident (e.g. trilinear cracking; linear cracking; 5-linear cracking) - Cracks with different lengths and with thicknesses larger than 1 mm - Severe plaster detachment in the wall-frame interfaces - Evident OOP detachment of the wall from the surrounding frame
	Collapse (Damage state 4)	- Partial collapse of parts of the walls in the case of panels with openings - Total collapse of the wall in the case of panels without openings

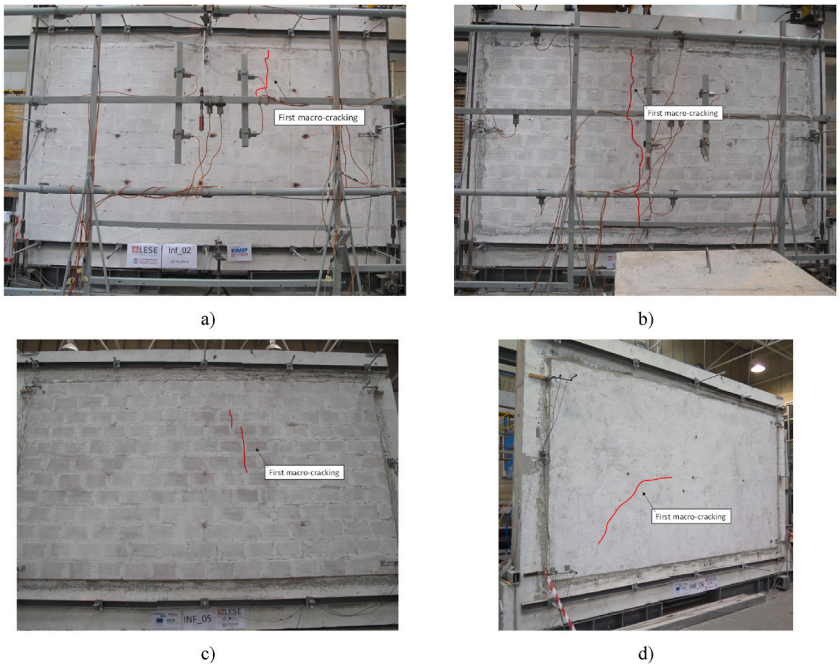

Fig. 7. First cracking (damage state 1): a) Inf_02; b) Inf_04, c) Inf_05 and d) Inf_06.

before, the first crack corresponds to the instant from which the stiffness starts to degrade. Thus, it is imperative to analyze the OOP drift for each specimen's first crack.

3.1.2. Damage state 2

The damage state 2 became evident during all the tests since it consisted of developing longer thin cracks. The extension of the first crack was observed, reported in damage state 1, in all the specimens. Most of the new cracks were due to the beginning of the OOP detachment of the wall from the surrounding frame (typically in the top wall-beam interface). Moreover, slight plaster detachment was also visible in the wall-frame interfaces due to the panel's relative OOP rotation or detachment. It is essential to mention that the

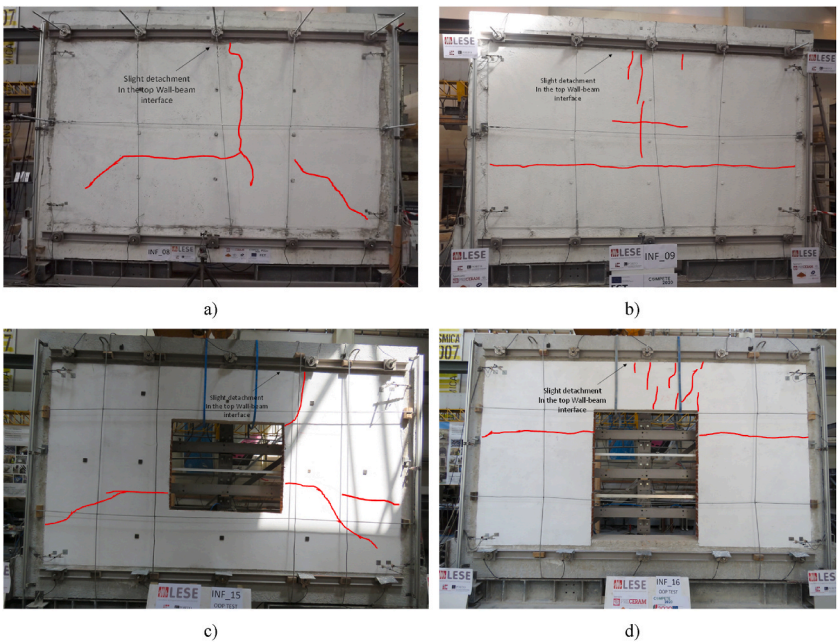

Fig. 8. Moderate damage (damage state 2): a) Inf_08; b) Inf_09, c) Inf_15 and d) Inf_16.

identification of the panels' OOP detachment consisted of the in-situ observations during the test and complementing with the displacement measurements from sensors located in the panel boundaries.

Fig. 8 presents some examples of infill walls with a moderate damage state, herein called damage state 2. For example, when the specimen Inf_08 reached an OOP drift of 0.11%, it was reported a first horizontal crack at the panel mid-span and mid-height. In the subsequent target displacements, there was not any significant evolution of the panel damage. Thus, when the OOP drift of 1.09% was achieved, sudden slight detachment of the wall from the top beam (up to 1 cm at the wall mid-length) occurred. The vertical crack emerged at the exact moment intercepting the first existing crack. In Fig. 8a, it is possible to observe additional diagonal cracks, one on each side of the wall, related to the arching-mechanism development. Future investigations are planned to be performed to study the effect of boundary conditions on the infill walls OOP behaviour.

Part of the damages observed can be due to the arching mechanism development, which is different if the panel is three or four borders constrained. In addition, the damage observed in the case of a pure OOP sliding of the wall from the surrounding wall is different from a panel that develops an arching mechanism. There is a need for a methodology that can assess the condition of all the wall interface conditions. Recently, De Angelis and Pecce [46] proposed an interesting approach for assessing the wall interface conditions by carrying out local dynamic tests using accelerometers. The authors proposed a specific identification procedure in which it is possible to study the real constraints of the wall.

It can be noticed that besides the fact that walls Inf_08 and Inf_09 were constructed and tested with the same geometry, materials, and test setup, the cracks developed in damage state 2 are different (see Fig. 8a and b). The workmanship can play a role in the cracking pattern development during and OOP loading demand. Wall Inf_09, presented in Fig. 8b, shows a thin horizontal crack with a total length equal to the wall length. Again vertical cracks emerged from the top wall-frame interface towards the horizontal crack due to the slight OOP. The same behaviour was observed in the remaining specimens without openings.

Finally, Fig. 8c and d present the moderate damage of the specimens with openings Inf_15 (window) and Inf_16 (door), respectively. The first crack was horizontal and located next to the opening for different OOP drift demands in both specimens. The first crack was observed in the wall Inf_15 for an OOP drift two times higher than wall Inf_16, which can be justified by the more extensive opening area of the last one. No damage evolution was reported in the subsequent target displacements until the drift of 1.19% and 1.15% was reached by Inf_15 and Inf_16, respectively. At this moment, diagonal cracks emerged in the wall Inf_15 from the corners of the opening towards the wall corners. On the other hand, in the wall with a central door (Inf_16), a similar horizontal crack was observed on the opposite side of the opening where the first crack developed in damage state 1. It must also be stated that some vertical cracks in the top of the opening towards the top interface were visible in both walls. Damage state 2 can be considered the limit beyond which the wall is no more easily repairable. If significant detachment from the frame is observed, it is challenging to repair the wall without demolishing it.

3.1.3. Damage state 3

The extensive damage state (damage state 3) corresponds to the situation in which the cracking pattern of the wall is evident (e.g. trilinear cracking; linear cracking; 5-linear cracking). It was possible to observe cracks with different lengths and with thicknesses larger than 1 mm in this stage. Most of these cracks were developed in the previous damage states but with a higher thickness, and it was pretty evident even in the zero-force step (after the OOP loading discharge). Severe plaster detachment in the wall-frame interfaces was observed due to the pronounced OOP detachment of the wall from the surrounding frame. The most conditioning factor in this

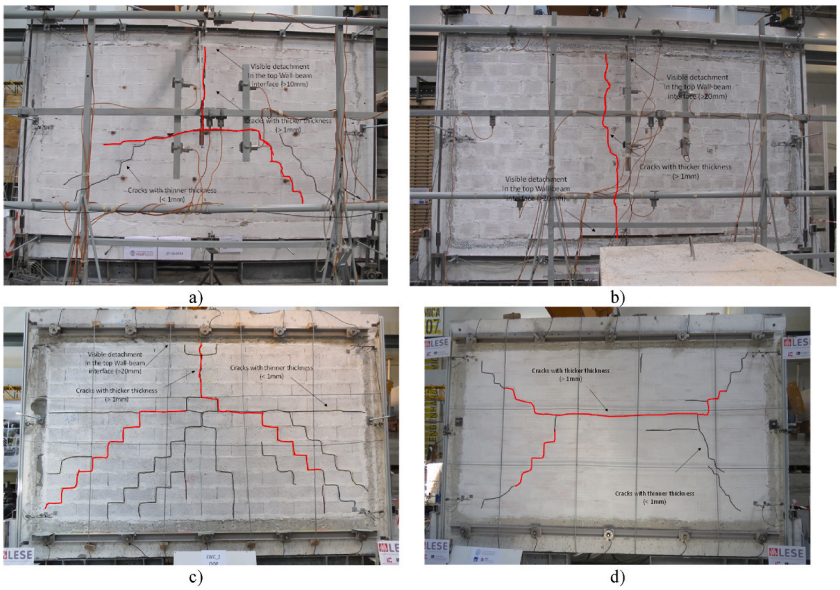

Fig. 9. Extensive Damage (damage state 3): a) Inf_02; b) Inf_04, c) LWC_OOP and d) AB_OOP.

damage state was the noticeable OOP detachment of the wall (larger than 10 mm relatively to the envelope RC frame).

Fig. 9 shows some examples of observed extensive damages. In the specimen Inf_02 (Fig. 9a), it is possible to observe the trilinear cracking pattern (red lines), typical of a wall three borders constrained. Also, the significant OOP detachment of the wall in the top interface agrees with this cracking pattern. Some other thinner cracks (black lines) were reported but with no significant meaning.

The extensive damage state of the specimen Inf_04 is presented in Fig. 9b. A bilinear crack was pretty pronounced due to the detachment of the wall in the top and bottom interfaces (>20 mm). In panel LWC_OOP, shown in Fig. 9c, the trilinear crack was again observed related to its OOP detachment in the top interface. It seems that there is a direct relationship between a possible OOP detachment of the panel along the different interfaces and the consequent cracking pattern (detachment in the top interface causes trilinear crack and in both top and bottom interfaces causes bilinear crack).

Finally, in the specimen AB-OOP, the detachment of the panel was not observed besides the development of the 5-linear cracking (see Fig. 9d) or other small cracks. This absence of detachment allowed to behave as a panel with four borders constrained.

3.1.4. Damage state 4

The realization of OOP tests up to the masonry infill walls collapse is fundamental to understand their actual deformation capacity and collapse mechanism. However, it is pretty challenging to perform this type of test due to the risk of damaging equipment and safety and economic reasons. The collapse of the walls was only achieved in specimens Inf_08, Inf_09, Inf_16 and AB-OOP, as can be observed in Fig. 10. The walls Inf_08 and AB-OOP did not collapse over the laboratory floor because of the safety steel cables used to prevent this phenomenon without affecting the OOP test (i.e. the steel cables were always distanced from the wall during the test).

Inf_08 and Inf_09 reached a similar collapse mechanism since it was a combination of a trilinear cracking plus the OOP detachment in the top and bottom interfaces. This simultaneous OOP detachment at both interfaces occurred when the vertical crack extended to the bottom of the wall, quite evident in Fig. 10a and b. This vertical crack extension separated the bottom portion of the wall located below the diagonal cracks of the trilinear cracking into two parts.

The specimen Inf_15 (central door) started the collapse mechanism when the diagonal crack developed in the right top corner of the opening reached the wall corner. The separation of the top portion of the wall simultaneously with the contribution of the horizontal crack contributed to the drop of the wall OOP strength. Thus, the rotation of the top and bottom (right) wall portions relatively to the horizontal crack was developed. After that, the sudden OOP detachment of the wall occurred, causing its collapse, as shown in Fig. 10c.

Finally, the collapse of specimen AB-OOP (Fig. 10d) occurred when the crusing of the four corners of the wall happened. At the same time, a vertical crack emerged from the bottom interface towards the horizontal crack due to the OOP detachment of the bottom portion of the wall.

It must be stated that the Group 1 specimens were not tested until reaching the collapse (damage state 4) for protection of the instrumentation equipment. The specimen LWC_OOP (Group 4) was not tested until the collapse due to the limitation of the pneumatic actuators.

It should be remarked that the extensive damage does not include partial collapses beside the detachment of pieces of plaster since, after the failure of some parts of the wall, the global collapse occurs quickly. That was the reason why the partial collapse was included

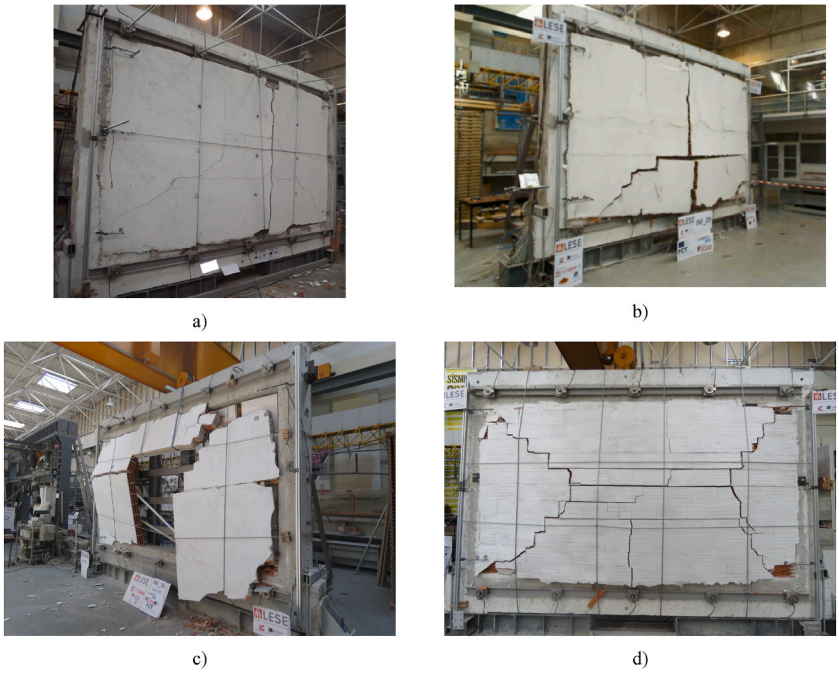

Fig. 10. Collapse (damage state 4): a) Inf_08; b) Inf_09, c) Inf_16 and d) AB-OOP.

in damage state 4.

In addition, it is also proposed a reference limit designated as the conventional failure of the wall. The conventional failure limit corresponds to a 20% strength reduction along the post-peak loading stage. The conventional failure is not considered a "damage state" since it does not correspond to specific wall damage. A similar approach is commonly adopted in the experimental testing of reinforced concrete elements (e.g. columns, beams). The conventional failure is often assumed, corresponding to a 20% strength drop. However, it must be stressed that the conventional failure stage in walls may not occur before their collapse (e.g. Inf_09, Inf_16). The fragile behaviour of the infill walls leads to the possibility of collapsing without any previous strength drop. Unfortunately, only a few tests were performed in the literature until the wall collapsed, which avoids comparing the collapse damage state and the conventional failure.

From the observation of the tests, it can be concluded that the damage corresponding to this stage was very similar to the damage observed in damage state 3, but with thicker cracks and with higher OOP detachment of the wall from the surrounding frame. It must be stated that since the masonry infill walls made of hollow masonry units are pretty fragile, sometimes the collapse of the walls can occur before the conventional point.

3.2. Damages versus out-of-plane drift demand

Following the definition of the different damage states, the OOP drift corresponding to the distinct damage states was identified to understand the effect of each variable on the damages observed in the masonry infill walls. Table 5 provides a data summary of the drift corresponding to each damage state. Results from specimens Inf_04 and LWC_OOP were considered in this analysis as outliers since they reached damage states for OOP drift demands quite different than the remaining specimens. Table 6 provides the Δdrift corresponding to each damage state by each specimen. This parameter represents the ratio between the OOP drift reached by the specimen and the OOP drift in which the maximum peak load was achieved. The main intention is to understand how far from the peak load each damage state occurs. Based on these results, it is possible to compare the damage observed in each wall and the corresponding OOP drift demand. In addition, it is plotted in Fig. 11 the OOP drift associated with each damage state. Based on these results, the following observations can be drawn, namely:

- The first cracking occurred in Group 1 between 0.11% and 0.47% (4.27 times higher), as shown in Fig. 11a. Reducing the panel support width caused the increment of the OOP drift demand necessary to develop the first crack. The reference specimen Inf_02 stands out significantly from the values recorded in the remaining specimens since it is 60%, 77% and 70% lower than the specimens Inf_04, Inf_05 and Inf_06, respectively. In Group 2, the OOP drift varied from 0.11% to 0.27% (2.36 times), justified by the openings as shown in Fig. 11b. For example, Inf_08 and Inf_09 (different workmanship) reached the first crack for almost the same OOP drift demand (0.11% and 0.12%, respectively). The openings lead to the delay of the first crack development. The panel with the largest opening area (i.e. Inf_16) reached the first crack for an OOP drift 2 times higher than Inf_15. The first crack observed in the panel LWC_OOP occurred for a drift of 0.29%, which is coherent with the other specimens. The Δdrift varies between 0.08 and 0.33 with a Coefficient of Variation (CoV) relatively smaller than the one observed in Table 5 (48.30% and 55.55%, respectively);

Regarding Group 2, moderate damage occurred for approximated OOP drift values (1.09%–1.69%). However, the highest OOP drift reached by AB-OOP can be related to the thinner thickness of the wall (110 mm) instead of the remaining specimens with 150 mm. Since it is possible to observe that the variation of the four other specimens ranged between 1.09% and 1.21%. Finally, moderate damage was reported in the wall LWC_OOP for an OOP drift of 0.45%, which is significantly lower when compared with the remaining walls (see Fig. 11c). This difference can be justified because the wall was built with a different type of masonry unit.

Table 5
Data summary concerning the drift corresponding to each damage state.

Specimen	Drift corresponding to damage state 1 (%)	Drift corresponding to damage state 2 (%)	Drift corresponding to damage state 3 (%)	Drift corresponding to damage state 4 (%)	Conventional Failure (%)
Inf_02	0.11	1.13	2.49	N/A[2]	3.91
Inf_04	0.28	0.63	3.56	N/A[2]	0.69
Inf_05	0.47	1.30	1.91	N/A[2]	N/A[1]
Inf_06	0.37	1.39	2.62	N/A[2]	N/A[1]
Inf_08	0.11	1.09	2.02	3.20	N/A[3]
Inf_09	0.12	1.21	2.34	2.58	N/A[3]
Inf_15	0.26	1.19	2.10	N/A[2]	3.92
Inf_16	0.13	1.15	1.95	3.24	3.24
AB-OOP	0.27	1.69	2.78	3.83	N/A[1]
LWC_OOP	0.29	0.45	2.20	N/A[2]	6.94
Range Values*	[0.11–0.47]	[1.09–1.69]	[1.91–2.78]	[2.58–3.83]	[3.24–3.92]
Mean	0.23	1.27	2.28	3.21	3.74
CoV	55.55%	14.43%	13.53%	13.77%	53.28%

N/A[1] – Not applicable since it did not occur a 20% reduction of the panel OOP maximum strength (post-peak stage).
N/A[2] – Not applicable since it did not occur panel OOP collapse.
N/A[3] – Not applicable since the collapse happened before a 20% reduction of the panel OOP maximum strength.
* – Not considering the results of the outliers Inf_04 and LWC_OOP.

Table 6
Data summary concerning the Δdrift corresponding to each damage state.

Specimen	Δdrift corresponding to damage state 1	Δdrift corresponding to damage state 2	Δdrift corresponding to damage state 3	Δdrift corresponding to damage state 4	Δdrift corresponding to conventional failure
Inf_02	0.08	0.78	1.73	N/A[2]	2.72
Inf_04	0.19	0.44	2.47	N/A[2]	1.10
Inf_05	0.33	0.90	1.33	N/A[2]	N/A[1]
Inf_06	0.26	0.97	1.82	N/A[2]	N/A[1]
Inf_08	0.08	0.76	1.40	2.22	N/A[3]
Inf_09	0.08	0.84	1.63	1.79	N/A[3]
Inf_15	0.18	0.83	1.46	N/A[2]	1.43
Inf_16	0.09	0.80	1.35	2.25	2.35
AB-OOP	0.19	1.17	1.93	2.66	N/A[1]
LWC_OOP	0.08	0.78	1.73	N/A[2]	1.66
Range Values*	[0.08–0.33]	[0.44–1.17]	[1.33–2.47]	[1.79–2.66]	[1.10–2.72]
Mean	0.17	0.78	1.66	2.23	1.85
CoV	48.30%	29.99%	19.86%	13.77%	32.26%

N/A[1] – Not applicable since it did not occur a 20% reduction of the panel OOP maximum strength (post-peak stage).
N/A[2] – Not applicable since it did not occur panel OOP collapse.
N/A[3] – Not applicable since the collapse happened before a 20% reduction of the panel OOP maximum strength.
* – Not considering the results of the outliers Inf_04 and LWC_OOP.

- The moderate damage was achieved in Group 1 for OOP drift values between 0.63% (Inf_04) and 1.39% (Inf_06). Considering all the data results, the moderate damage observed in Inf_04 occurred for a low OOP drift. Again, if we look at the conventional failure, it happened for a similar drift (0.69%). It is important to remember that during the OOP test of the wall Inf_04, a pure vertical crack suddenly occurred with an OOP detachment in the top and bottom interfaces of the wall. This behaviour may have had some relationship with applying the axial load in the envelope RC columns that could have compressed the infill wall and modified the OOP response. Since the behaviour of Inf_04 was significantly different from the remaining walls, it will be analyzed separately from the remaining.

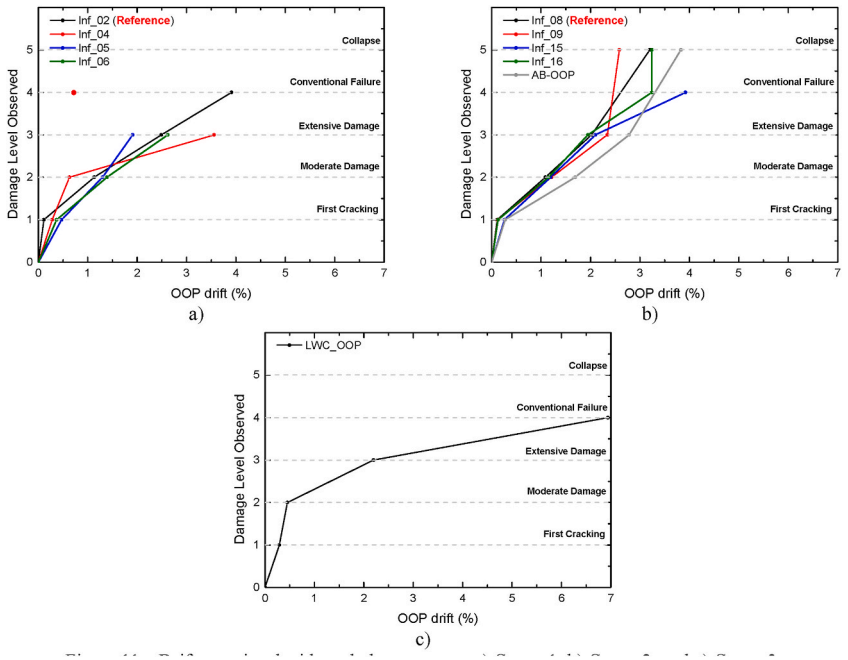

Fig. 11. Drift associated with each damage state: a) Group 1; b) Group 2, and c) Group 3.

In this damage state, it is possible to observe that the Δdrift ranges between 1.33 and 2.47, with a mean value of 1.66 and a CoV equal to 19.86%;

- The extensive damage was reached in Group 1 for OOP drift demands between 1.91% (Inf_05) and 3.56% (Inf_04). In Group 2, it was observed that the extensive damage state was observed for OOP drift demands between 1.95% (Inf_16) and 2.78% (AB-OOP). The last specimen, LWC_OOP from Group 3, reached this damage state for similar OOP drift (2.2%). The Δdrift ranges between 0.44 and 1.17, with a mean value of 0.78 and a CoV equal to 29.99%;

- The conventional failure was only reached for specimens Inf_02, Inf_04, Inf_15 and LWC_OOP. As proved by the range between 0.69% (Inf_04) and 6.94% (LWC_OOP), significant dispersion of results was found. On the one hand, the lowest result can be justified by the axial load on the columns. The red circle observed in Fig. 11a is the result reached by Inf_04. On the other hand, the most extensive OOP drift of 6.94% reached by LWC_OOP can be due to the significant thickness of this specimen (>300 mm), preventing a sudden decrease of the OOP strength. Regarding the Δdrift, it ranges from 1.10 to 2.72 with an average of 1.85;
- Finally, the OOP collapse occurred in the testing of walls Inf_08, Inf_09, Inf_16 and AB-OOP. The collapse happened for the specimen Inf_09 for a drift of 2.58% and a most considerable drift in specimen AB-OOP (3.83%), about 1.48 times.

Moreover, the information herein collected is essential to define OOP drift intervals. The different damage state levels can be observed in masonry infill walls subjected to pure OOP loadings. This novel information can help support future investigations. The drift variation (i.e. minimum and maximum value) OOP drift results for each damage state level was observed and aggregated in Fig. 12. This Figure shows the range values considering the contribution of all specimens excluding outliers Inf_04 and LWC_OOP. It can be seen that: the first cracking occurred for OOP drift values ranging from 0.11% to 1.09%; moderate damage between 1.09% and 1.91%; extensive damage between 1.91% and 2.78%; conventional failure between 3.24% and 3.92% and collapse between 2.58% and 3.83%. Please note that damage level 1 was observed between 0.11% and 0.47%, but damage level 2 was only observed for drifts higher than 1.09%. Thus, it was extended the drift range related to damage level 1 until 1.09%. The same assumption was performed to the moderate damage (the upper drift limit was shifted to 1.91%).

3.3. Damages versus force-displacement curves

It is crucial to correlate the damage state reached by each infill wall and its force-displacement curve. These correlations are important to define the infill limit states in terms of positioning on the force-displacement curves, which is the most general method for assessing the level of damage (e.g., for externally strengthened infills where the damage is not very visible). Through the comparison between the damage states and the force-displacement curves, shown in Fig. 13, the following considerations can be drawn:

- the first cracking corresponds to the first drop of the panel OOP stiffness (e.g. Inf_02, AB-OOP, Inf_16) and sometimes to a slight strength drop (e.g. Inf_04, Inf_05);
- moderate damage corresponds to the peak load in specimens Inf_04 and Inf_02, but in the remaining ones, it appears like an intermediate stage until reaching the OOP maximum strength, whereas the cracking pattern is starting to be observed with slight OOP detachment (one interface) of the wall and thinner cracks;
- extensive damage is usually associated with the peak loading stage or stages pretty close to the peak loading stage, and it corresponds to a significant OOP detachment of the wall and thicker cracks;
- Collapse represents the total OOP strength loss.

4. Pilot application of a damage index quantification for masonry infill walls made with hollow clay horizontal bricks

4.1. Methodology description

As investigated by different authors, the structural damage induced by seismic actions can be quantified to assess the structure relative to a pre-defined set of limit states [47–50]. Damage indexes are generally divided into two categories: local and global. Local indexes are usually calibrated for a specific structural or non-structural member [51]. On the other hand, global indexes are used to predict the failure of a complete building structure. They are usually computed as a weighted combination of local damage indices of individual members [52].

The goal for an optimum damage assessment method should be its ability for general applicability, i.e., it must be able and valid for

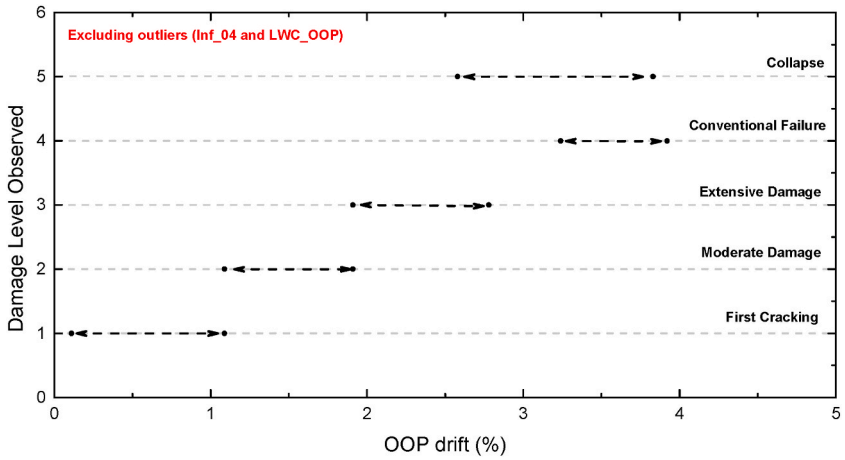

Fig. 12. Drift range obtained from the experimental tests (excluding outliers Inf_04 and LWC_OOP).

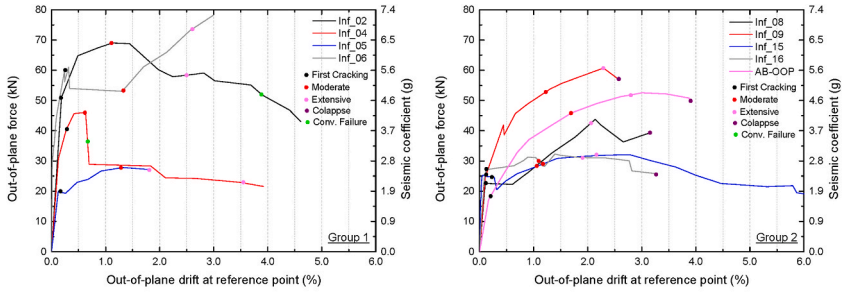

Fig. 13. Force-displacement curves versus damage states: a) Group 1 and b) Group 2.

a set of structural systems based on a simple formulation to generate easily interpretable results consequently. The development of damage quantification methods for infill walls under pure OOP loadings considering the hysteretic energy dissipation was not yet approached in the literature. Nevertheless, in general, there are methods to quantify OOP (or IP/OOP) damage states based on displacement domains [31].

The practical usefulness of a damage index (DI) model is to provide an insight concerning the damage state of walls based on the OOP displacement, energy dissipation and maximum strength. The proposed DI model is based on the damage evolution of infill walls tested under OOP loadings and can be used to assess the damage condition of walls simulated using detailed micro-modelling or simplified macro-modelling approaches. It can also be very useful for calibrating the hysteretic OOP behaviour of the numerical models.

As it can be learned from the literature, damage indexes can be classified as cumulative or noncumulative. Noncumulative indexes relate the state of damage to peak response quantities and do not account for cyclic loading effects. Cumulative indices include part or all of the loading history to predict the capacity reduction due to cyclic repetitive loading. The following reviews of damage indexes can only be found in the literature dedicated to reinforced concrete structures [53,54].

The methodology to compute the DI is adapted from the method proposed by Park and Ang [55]. The DI is defined by a linear combination of the normalized maximum deformation and the normalized dissipated hysteretic energy resulting from cyclic loading. The DI is therefore expressed by Equation (1):

$$DI = \frac{d_{max}}{d_u} + \beta \frac{\int dE}{F_{max} d_u} \tag{1}$$

Where d_{max} is the maximum OOP displacement reached in each loading cycle and d_u is the maximum OOP displacement reached by the wall. $\int dE$ is the area of the dissipated energy and F_{max} is the maximum OOP strength predicted for the infill wall, and can be estimated using Equation (2). Finally, β is the degradation parameter representing the influence of cyclic response on the damage. The DI range values vary from 0 to greater than 1 (being at the end of the test $d_{max}/d_u = 1$ and therefore DI = 1+something). The total damage (collapse) is assumed when DI $\geq$ 1. The proposed DI is based on the original Park and Ang [51] proposal. The authors suggested to use an analytical equation to estimate F_{max}. Thus the calibration of the DI based on analytical expressions may allow the use of this approach in the absence of experimental data. Concerning Equation (2), the authors understand the reviewer's point of view. They agree that this expression is mainly useful for vertical arch mechanisms. Nevertheless, this equation also seems to predict the maximum strength of the tested walls well. Other expressions can be used to estimate the maximum strength more accurately for other walls with other expected failure mechanisms (e.g. double-arching mechanism). Future calibrations must be performed using other prediction equations to estimate the Fmax of infill walls with different failure modes.

The methodology adopted to compute the DI model comprises five steps, as described below:

i) d_{max} is determined in each cycle;
ii) d_u is defined as the maximum OOP displacement reached by the wall;
iii) $\int dE$ is computed;
iv) F_{max} is computed based on the analytical model Eurocode 6 [56] proposed to estimate the OOP strength of masonry walls or infills, respectively, without strengthening strategies. This model suggests that the maximum OOP distributed load (q_{max}) can be estimated based on a one-way (vertical) arch resisting mechanism. Thus the maximum horizontal uniformly distributed load (q_{max}) can be defined as in Eq. (2). Then the F_{max} was estimated, taking into account the maximum distributed load q_{max} and the panel area;

$$q_{max} = f_{mv} \left(\frac{t_w}{H_w}\right)^2 \tag{2}$$

v) β is adjusted to fit with damage observations (e.g. the collapse only occur for DI $\geq$ 1).

Finally, it must be underlined that the wall hysteretic behaviour causes damage. Part of this damage is directly proportional to the

wall displacement, i.e. $\frac{d_{max}}{d_u}$, and the other part is proportional to the energy dissipation (i.e. $\frac{\int dE}{F_{max} d_u}$). The β is used to weigh the energy dissipation effect on the damage quantification.

4.2. Discussion of the results

The damage index was computed from the OOP test results (LWC_OOP and Inf_04 were excluded). For each masonry infill wall, the β estimated is presented in Table 7 In addition, the global average β and its coefficient of variation were computed and presented in the end of the table.

The results are plotted in Fig. 14 in terms of DI evolution during the cyclic tests. The corresponding drift for each damage state observed during the tests (reported in the previous section) is presented in the DI curves. The DI values plotted in Fig. 14 were obtained with the specific β values that were calibrated and that are presented in Table 7.

From these results, it is possible to observe that the first cracking of the walls occurred for DI between 0.03 and 0.21. The moderate damage state was reached for DI values between 0.15 and 0.56, the extensive damage ranging from 0.26 to 1.04. The collapse occurred for DI values upper than 1. Based on this, the following damage index range values for each specific damage state are herein proposed: first cracking $0 < DI \leq 0.25$; moderate damage $0.25 < DI \leq 0.60$; extensive damage $0.60 < DI \leq 1$ and collapse $DI \leq 1$.

The average value obtained for the β is 0.046 with a CoV of 29.56%. Nevertheless, the determination of the β parameter would benefit from more tests to reduce the coefficient of variation and effect of a high number of variables. However, this is the first proposal for a DI model for masonry infill walls. The β parameter found can be used in future simulations of masonry infill walls made of hollow clay horizontal bricks subjected to pure OOP loadings. Future works are needed to validate the β values herein proposed and compute β values for masonry infill walls with different characteristics (i.e. masonry units, boundary conditions, among others).

5. Energy dissipation and equivalent viscous damping

5.1. Cumulative and normalized energy dissipation

The cumulative energy dissipation in each masonry infill wall can be computed as the internal area of the OOP force-drift response curve. The cumulative energy dissipation was computed according to Equation (3). This response parameter allows to analyze the ability of the infill walls to dissipate the energy induced by the seismic action. The influence of each parameter in the energy dissipation capacity is not well covered and discussed in the literature since, as previously stated, a large part of the existing data results are related to monotonic tests.

$$E_{cum} = \int F_{OOP} d_{OOP} \tag{3}$$

F_{OOP} is the infill wall OOP strength and d_{OOP} is the wall OOP displacement at the reference point.

From the analysis of results obtained from the testing of group 1 specimens (Fig. 15a), it can be observed that the use of plaster (Inf_06) did not contribute directly to the increase of the energy dissipation capacity. On the contrary, it was observed that for OOP drift between 1 and 2.7%, the dissipation capacity of the reference specimen was higher by about 10%. The reduction of the panel width support (Inf_05) and axial load application on the envelope columns (Inf_04) resulted in a substantial decrease in the energy dissipation capacity. For OOP drift lower than 1%, the reduction ranged between 10 and 45%. For OOP drift larger than 1%, the reduction ranged between 40% up to 75%. This reduction of the energy dissipation capacity is expected since the arching mechanism development is affected by a lower support widht. Only 2/3 of the panel thickness can bend, reducing the panel strength and energy dissipation as expected.

From the analysis of results obtained from the testing of group 2 specimens (Fig. 15b), it can be seen that the workmanship (Inf_09) can affect this response parameter. In this case, the infill wall made by different labour dissipated higher energy by about 57% for an OOP drift of 0.66%, 80% for an OOP drift of 0.89%, 68% for an OOP drift of 1.31% and 43% for an OOP drift of 2.14%. Again, since the workmanship is not a “controlled parameter”, it seems that despite the same arrangement of the brick units and the same methodology

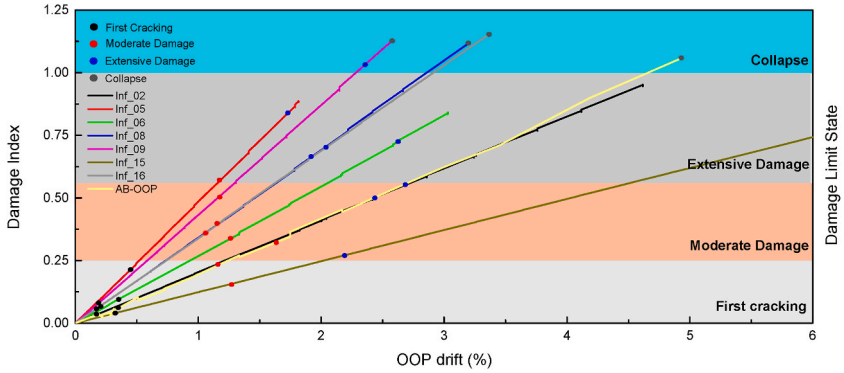

Fig. 14. Drift range obtained from the experimental tests (excluding outliers Inf_04 and LWC_OOP).

Table 7
β parameter assumed to calculate the damage index.

Specimens	β
Inf_02	0.046
Inf_05	0.068
Inf_06	0.039
Inf_08	0.061
Inf_09	0.045
Inf_15	0.026
Inf_16	0.055
AB-OOP	0.03
Average	0.046
CoV (%)	29.56

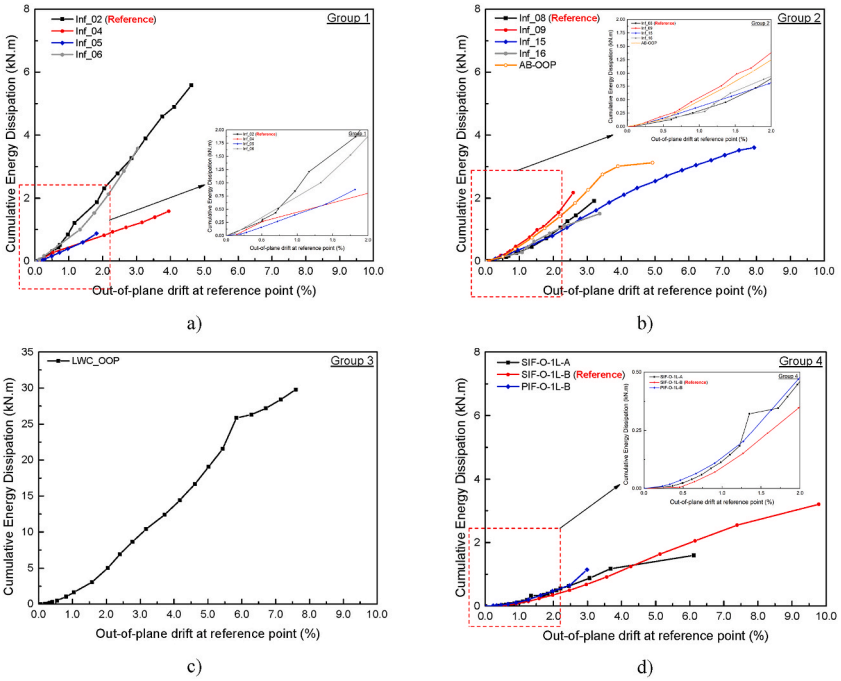

Fig. 15. Cumulative energy dissipation a) Group 1; b) Group 2; c) Group 3 and d) Group 4.

for preparing the mortar, it does not reflect the same strength and energy dissipation capacity. The operator technique may affect this response parameter beyond experimental variability.

The use of a thinner hollow clay horizontal brick unit (AB-OOP) also increased the infill wall's energy dissipation capacity by about 30% for low OOP drift and up to 60% for higher OOP drift. As can be seen, from the cracking pattern it seems that the two way arching activated for thinner this thinner pannel and not for the thicker ones. This two-way arching contributed to a higher strength and energy dissipation capacity.

Concerning the effect of the openings, it seems that the dissipation capacity was only affected for OOP drift higher than 2%. The openings reduced the energy dissipation capacity by about 5–15% for the same displacement demands. For OOP drift lower than 2%, the specimens with openings dissipated higher energy between 10 and 37%. Nonetheless, it must be stressed that a higher number of tests are still required for investigating the effect of the opening.

During the test of specimen LWC_OOP, plotted in Fig. 15c, it can be observed that for OOP drift levels lower than 5.7%, the wall energy dissipation increases highly than for drift levels higher than 5.7%. The failure mode that occurred for this level of drift (masonry unit crushing and sliding between portions of the wall as described in Ref. [34]) reduced the energy dissipation capacity of the wall.

Finally, in the specimens from Group 4, it can be found that the energy dissipation capacity is very similar until the OOP drift of 2% (Fig. 15d). After that, the specimen with a central window (PIF–O-1L-B) dissipated 67% higher energy than the reference specimen for the OOP drift of 3%. This result was not observed, for example, in Group 2. The effect of the openings in the energy dissipation capacity needs further investigation by performing additional OOP tests (preferable) or using finite element modelling analysis. As observed in Group 2, the workmanship leads to a variation of the energy dissipation between 18% and 29%.

For each specimen, the energy dissipation determined as shown above was normalized with the total dissipated energy until the yield point (E_y), and are plotted in Fig. 16. For each group, the best-fit polynomial or power correlation curve is proposed. The yield

point was computed according to the Eurocode 8 [57] proposal (Annex B.3, equation B.6). This point is calculated by ensuring that the internal areas of the actual and the idealized force-displacement curves are equal. The intersection point between those curves gives the yield point of the wall. The OOP displacement ductility was computed as the ratio between the actual and the yielding displacement. In the end, Fig. 16e presents an equation that fits all specimens' results.

In Fig. 16a it is shown the results from Group 1 in which can be noticed that the specimen Inf_05 reached higher normalized energy dissipation (about 1.1–1.5 times higher than the reference one), and the specimen Inf_04 the lower one (−20% to- 70% than the reference specimen. The specimen Inf_06 reached normalized energy dissipation values slightly lower than the reference specimen for the same OOP ductility demand (−5% to −20%). Equation (4) is proposed to fit the data results from all the group 1 specimens with an R^2 of 0.82. It can be seen that the results reached by the specimen Inf_04 and Inf_05 (for higher OOP ductility demands) contribute to a lower R^2.

In Fig. 16b it is shown the results from Group 2. The specimen Inf_15 dissipated higher energy normalized (5%–25% higher than the reference specimen) for OOP ductility demands lower than 7. The specimens Inf_08 and the AB-OOP dissipated high normalized energy (1.2–1.45 times higher than Inf_09) for OOP drift demands higher than 7. Equation (5) is proposed as the best-fit power curve for the specimens of group 2 with a good approximation ($R^2 = 0.93$).

Regarding Group 3, presented in Fig. 16c, a similar curve shape like the one observed in the cumulative energy dissipation response was obtained as expected (Fig. 16c). Equation (6) is proposed considering the single response of wall LWC_OOP with a very high approximation as expected ($R^2 = 0.98$).

$$\frac{E_{cum}}{E_y} = 0.0071 \times \mu^3 - 0.0061 \times \mu^2 + 1.326 \times \mu \tag{4}$$

$$\frac{E_{cum}}{E_y} = 0.4789 \times \mu^{1.4272} \tag{5}$$

$$\frac{E_{cum}}{E_y} = 0.7645 \times \mu^{1.82} \tag{6}$$

$$\frac{E_{cum}}{E_y} = 0.0635 \times \mu^2 + 2.0011 \times \mu - 1.0282 \tag{7}$$

In Fig. 16d it is shown the results from Group 4. The specimens have a similar response for ductility levels up to 2. After that, the specimens SIF–O-1L-A and PIF-O-1L-P dissipated high normalized energy than the reference specimen SIF–O-1L-B between 1.08 and 1.59 times. Equation (7) is proposed with a considerable approximation, namely an $R^2 = 0.91$.

The combination of the low number of tests with the high number of parameters understudies in these experimental tests impacted the accuracy of the equations proposed to estimate the evolution of the viscous damping. These equations can be used as a reference to compare with the results from future numerical investigations that can be carried out to investigate the OOP behaviour of masonry infill walls, and the effect of each variable on this response parameter.

5.2. Equivalent hysteretic viscous damping

The OOP equivalent hysteretic viscous damping of masonry infill walls was not covered yet in the existing studied in the literature. As mentioned before, this can be justified because a large part of the tests performed was monotonic.

For each database specimen, the equivalent hysteretic viscous damping (ξ_{hyst}) was computed according to Equation (8). This parameter depends on the relationship between the displacement ductility demand and its energy dissipation capacity. The determination of this parameter started with identifying the delimitation by each pair of zero-force points for each half-cycle (i.e. charge-discharge for each target displacement). After that, for each force-displacement half-cycle, the maximum force reached (i.e. F_{max}) and the maximum displacement (i.e. D_{max}) were evaluated, allowing to calculate the strain energy. Therefore, the dissipated energy was computed by calculated for each force-displacement half-cycle. Finally, the equivalent hysteretic viscous damping (ξ_{hyst}) was calculated using Equation (8).

The equivalent hysteretic viscous damping was computed for all the specimens according to the procedure described below. After that, all the specimens of each group were aggregated and presented in Fig. 17. The best logarithmic curve that fits with the results of each group found out. From the analysis of the results obtained for the equivalent viscous damping function of OOP displacement ductility, it is possible to verify that:

- It can be observed that the best approximation was obtained for Group 4 (Equation (12)) with an $R^2 = 0.72$ and the lowest one for Group 1 (Equation (9)) with an $R^2 = 0.45$;
- A more significant dispersion of the results in Group 1, shown in Fig. 17a, which can mean that the reduction of the panel support conditions and the existence of axial load in the envelope RC columns affects this response parameter directly. On the other hand, the (reference) specimen Inf_02 and the Inf_06 reached similar results;
- In Group 2, the parameter that affected the correlation of Equation (10) is the opening, since the results of specimens Inf_15 (central window) and Inf_16 (central door) are the ones furthest away from the proposed logarithmic line, as shown in Fig. 17b;

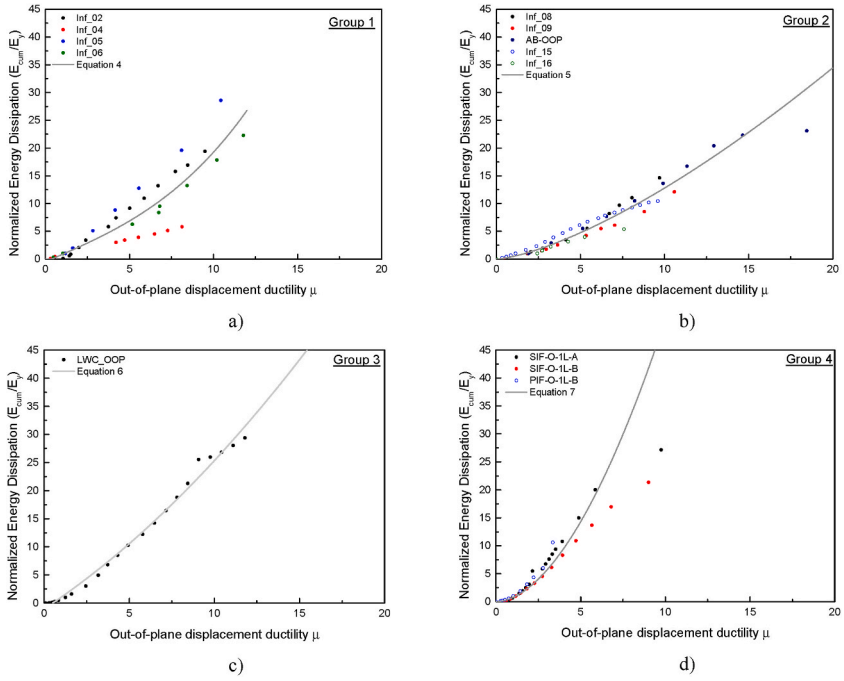

Fig. 16. Normalized energy dissipation a) Group 1; b) Group 2; c) Group 3; and d) Group 4.

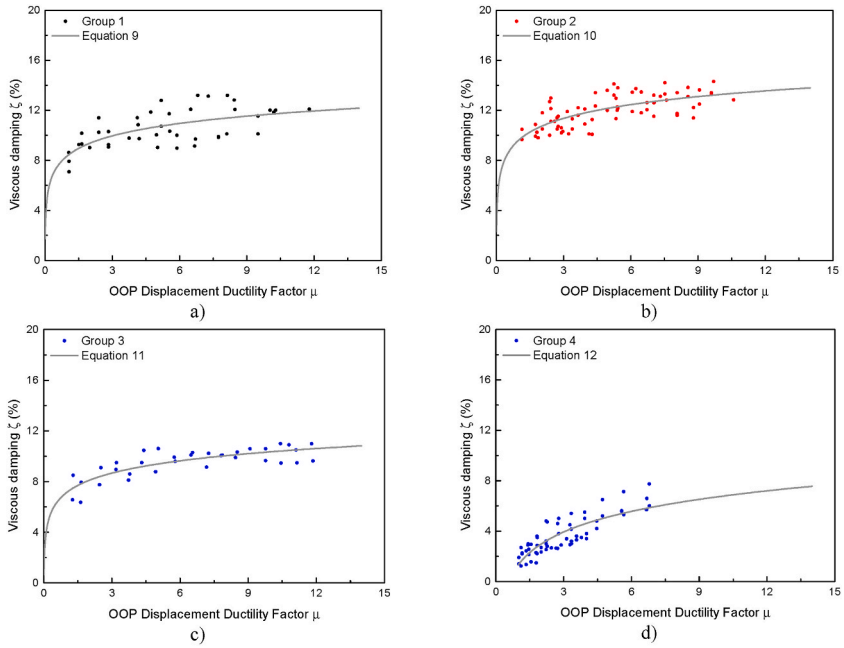

Fig. 17. Equivalent viscous damping a) Group 1; b) Group 2; c) Group 3; and d) Group 4.

- The result from LWC_OOP (Group 3) is plotted in Fig. 17c, in which is visible the different value of the viscous hysteretic damping in the first and second half-cycle for each target displacement. The proposed Equation (11) reached the second-best approximation with an $R^2 = 0.67$;

$$\xi_{hyst} = \frac{A_{half-cycle}}{2\pi F_{max} D_{max}} \tag{8}$$

$$\xi_{hyst,Group1} = 1.4372 \times \ln(\mu) + 8.3745 \quad (9)$$

$$\xi_{hyst,Group2} = 1.5869 \times \ln(\mu) + 9.6113 \quad (10)$$

$$\xi_{hyst,Group3} = 1.3995 \times \ln(\mu) + 7.1332 \quad (11)$$

$$\xi_{hyst,Group4} = 2.3542 \times \ln(\mu) + 1.3473 \quad (12)$$

The good approximation obtained for Group 4 is primarily due to the close results obtained by the specimens SIF–O-1L-A and SIF–O-1L-B (Equation (12)), as shown in Fig. 17d. Again, the effect of the opening contributed to reducing the R^2 to 0.72.

6. Final remarks

The study of the OOP behaviour of masonry infill walls has been the focus of numerous studies during the last years. Most of the studies available in the literature concerning the masonry infill walls' OOP behaviour cover their experimental response in terms of damage evolution, force-displacement, maximum strength and deformation capacity of the walls. However, none of them proposes a specific damage index for walls subjected to OOP loadings or discusses their hysteretic viscous damping, which is justified by the fact that many of those tests were carried out fundamentally applying a monotonic OOP load, not provoking the walls to collapse. However, it is fundamental to increase the knowledge concerning their non-linear behaviour when subjected to cyclic loadings.

Based on this motivation, the primary purpose of this manuscript was to provide the first proposal of damage states for masonry infill walls subjected to OOP loadings. After that, a pilot damage index model was proposed for masonry infill walls made of hollow clay horizontal brick units. The third objective of this work was the assessment and discussion of their normalized energy dissipation capacity and their hysteretic viscous damping. Some analytical formulations were proposed to estimate these parameters. An empirical-based approach was used to estimate the formulations proposed. A database containing the results of thirteen OOP tests performed by three different authors was used to achieve these goals.

Regarding the damage states proposed for masonry infill walls subjected to OOP loadings, four damage states are proposed, namely: first cracking (damage state 1); moderate damage (damage state 2); extensive damage (damage state 3) and collapse (damage state 4). These damage states are proposed based on observing the damage evolution of the OOP response of the infill walls. It was evident that the damage states are directly related to the force-displacement curve, namely: i) the first crack represents the first drop of the panel OOP strength and/or stiffness; ii) moderate damage corresponds to an intermediate stage until reaching the OOP maximum strength where the cracking pattern is starting to be observed with slight OOP detachment (one interface) of the wall and thinner cracks; iii) extensive damage is usually associated to the peak load stage with significant OOP detachment of the wall from the surrounding RC frame and thicker cracks; iv) total collapse represents the total OOP strength loss. The behaviour of masonry infill walls made of hollow clay horizontal bricks is pretty fragile with collapses without prior strength degradation. It was observed for this type of wall that the first cracking occurred for OOP drift values ranging from 0.11% to 1.09%; moderate damage between 1.09% and 1.91%; extensive damage between 1.91% and 2.78% and collapse between 2.58% and 3.83%. The conventional failure occurred between 3.24% and 3.92%, but in some cases the wall collapsed before dropping 20% of its OOP strength due to its fragile behaviour.

Moreover, a pilot application of a damage index (DI) model for masonry infill walls made of hollow clay bricks was carried out based on the proposal of Park and Ang [55]. Based on this proposal, it was observed that the first cracking ranged for a DI between 0 and 0.25, the moderate damage between 0.25 and 0.60, the extensive damage between 0.60 and 1 and the collapse for DI higher than 1. It was found an average value of 0.046 for β. Nonetheless, many questions are still open concerning the OOP behaviour of masonry infill walls, especially regarding the description and evaluation of the damage based on damage indexes. The DI herein proposed are only related to masonry infill walls made of hollow clay horizontal brick units. The large variations of the DI can be associated with the combination of many parameters studies and the low number of tests performed. The experimental variability may also affect the DI range for each damage state. Future complementary studies need to be performed using even more tests to support the proposals.

Concerning the normalized energy dissipation, it was found some dispersion of the results as expected. However, the analytical equation proposed for each group of specimens and all the infill walls achieved an interesting approximation ($R^2 > 0.89$). Besides, it was observed that the reduction of the panel width support and the openings could increase this parameter. The workmanship can introduce a variation between 8% and 21%.

Finally, the hysteretic viscous damping was analyzed and it was adjusted a logarithmic curve for each set of results. As proved by the low accuracy of the proposed logarithmic curves, large dispersion was found (lowest $R^2 = 0.45$; highest $R^2 = 0.72$). An analytical equation for fitting the specimens' data results (excluding group 4 due to the scale factor) resulted in This can be justified by the low number of tests, the large number of variables under study and the fragile and non-linear behaviour of the infill walls.

Nevertheless, it needs to be underlined that the conclusions and analytical formulations herein presented are the result of the analysis of only sixteen masonry infill walls with a rectangular shape (length higher than height), four borders constrained and made of hollow clay horizontal brick units (excluding one specimen made of a vertical hollow lightweight concrete block). It needs to be emphasized that this work aims to be a first proposal that approaches the damage states and viscous damping of masonry infill walls under pure OOP loadings. Thus, masonry infill walls with similar and different characteristics of those herein studied (i.e. support conditions, boundary conditions, openings and masonry units) need additional investigation (experimental and numerical) to validate the proposals and conclusions herein found. The need for an international database comprising data results from OOP cyclic tests and

their material and mechanical properties is high since it will help identify the parameters that still need to be investigated. Thus, a global overview will help advance the existing knowledge on their seismic behaviour and develop tools or guidelines for reducing their vulnerability.

The OOP behaviour of the masonry infill walls depends on several parameters and the existing number of tests is not sufficient to understand their real impact. For example, the effect of the workmanship is an important factor that affects the wall OOP seismic performance. Further investigations are needed to clarify the impact of those parameters and quantify the effect of experimental variability. Future complementary studies should also be carried out to support the conclusions herein found. Namely, detailed numerical simulations can be an interesting approach to circumvent the difficulties inherent in carrying out this type of experimental testing. Parametric studies will provide a detailed analysis of the effect of other parameters not covered in this study (e.g. walls with different geometries, different types of opening and positioning, among others).

Author statement

We declare that this manuscript is original, has not been published before and is not currently being considered for publication elsewhere. We confirm that the manuscript has been read and approved by all named authors and that there are no other persons who satisfied the criteria for authorship but are not listed. We further confirm that all have approved the order of authors listed in the manuscript of us. We understand that the Corresponding Author is the sole contact for the Editorial process. He is responsible for communicating with the other authors about progress, submissions of revisions and final approval of proofs.

Declaration of competing interest

The authors declare that they have no known competing financial interests or personal relationships that could have appeared to influence the work reported in this paper.

Acknowledgements

This work was financially supported by: Base Funding - UIDB/04708/2020 and Programmatic Funding - UIDP/04708/2020 of the CONSTRUCT - Instituto de I&D em Estruturas e Construções - funded by national funds through the FCT/MCTES (PIDDAC). This work was also supported by the Foundation for Science and Technology (FCT) - Aveiro Research Centre for Risks and Sustainability in Construction (RISCO), Universidade de Aveiro, Portugal [FCT/UIDB/ECI/04450/2020].

The authors would also like to express a special acknowledgement to the reviewers for their valuable suggestions that increased the manuscript quality.

References

[1] F. Luca, G.M. Verderame, F. Gómez-Martínez, A. Pérez-García, The structural role played by masonry infills on RC building performances after the 2011 Lorca, Spain, earthquake, Bull. Earthq. Eng. 12 (2014//2014).
[2] L. Hermanns, A. Fraile, E. Alarcón, R. Álvarez, Performance of buildings with masonry infill walls during the 2011 Lorca earthquake, Bull. Earthq. Eng. 12 (5) (2014) 1977–1997.
[3] A. Masi, et al., Seismic response of RC buildings during the mw 6.0 august 24, 2016 Central Italy earthquake: the amatrice case study" bulletin of earthquake engineering, journal article 17 (10) (October 01 2019) 5631–5654.
[4] G.M. Calvi, D. Bolognini, Seismic response of reinforced concrete frames infilled with weakly reinforced masonry panels, J. Earthq. Eng. 5 (2) (2001) 153–185. Article.
[5] M.T. De Risi, C. Del Gaudio, P. Ricci, G.M. Verderame, In-plane behaviour and damage assessment of masonry infills with hollow clay bricks in RC frames, Eng. Struct. 168 (2018) 257–275.
[6] A. Furtado, H. Rodrigues, A. Arêde, H. Varum, Out-of-plane behavior of masonry infilled RC frames based on the experimental tests available: a systematic review, *Construction and Building Materials,* Review 168 (2018) 831–848.
[7] F. Anić, D. Penava, L. Abrahamczyk, V. Sarhosis, A review of experimental and analytical studies on the out-of-plane behaviour of masonry infilled frames, Bull. Earthq. Eng. 18 (5) (2020/03/01 2020) 2191–2246.
[8] A. Mansouri, M.S. Marefat, M. Khanmohammadi, Experimental evaluation of seismic performance of low-shear strength masonry infills with openings in reinforced concrete frames with deficient seismic details, Struct. Des. Tall Special Build. 23 (15) (2014) 1190–1210.
[9] T.-C. Chiou, S.-J. Hwang, Tests on cyclic behavior of reinforced concrete frames with brick infill, Earthq. Eng. Struct. Dynam. 44 (12) (2015) 1939–1958.
[10] G. Blasi, F. De Luca, M.A. Aiello, Brittle failure in RC masonry infilled frames: the role of infill overstrength, Eng. Struct. 177 (2018/12/15/2018) 506–518.
[11] P.G. Asteris, Lateral stiffness of brick masonry infilled plane frames, J. Struct. Eng. 129 (8) (2003) 1071–1079. Article.
[12] X. Chen, Y. Liu, Numerical study of in-plane behaviour and strength of concrete masonry infills with openings, Eng. Struct. 82 (2015) 226–235.
[13] S. Surendran, H.B. Kaushik, Masonry infill RC frames with openings: review of in-plane lateral load behaviour and modeling approaches, *Open Construction and Building Technology Journal,* Review 6 (1) (2012) 126–154. SPEC.
[14] U.A. Siddiqui, H. Sucuoğlu, A. Yakut, Seismic performance of gravity-load designed concrete frames infilled with low-strength masonry, Earthquake and Structures 8 (1) (2015) 19–35.
[15] A. Furtado, H. Rodrigues, A. Arede, H. Varum, Experimental investigation on the possible effect of previous damage, workmanship and test setup on the out-of-plane behaviour of masonry infill walls, J. Earthq. Eng. (2021) 1–32.
[16] A. Furtado, H. Rodrigues, A. Arêde, H. Varum, Effect of the panel width support and columns axial load on the infill masonry walls out-of-plane behavior, J. Earthq. Eng. 24 (4) (2020) 653–681.
[17] L. Cavaleri, M. Zizzo, P.G. Asteris, Residual Out-Of-Plane Capacity of Infills Damaged by In-Plane Cyclic Loads, vol. 209, Engineering Structures, 2020. Art. no. 109957.
[18] F. da Porto, M. Donà, N. Verlato, G. Guidi, Experimental testing and numerical modeling of robust unreinforced and reinforced clay masonry infill walls, with and without openings," (in English), Original Research, Frontiers in Built Environment 6 (2020-December-10 2020), 204.
[19] F. Anić, D. Penava, I. Guljaš, V. Sarhosis, L. Abrahamczyk, Out-of-plane cyclic response of masonry infilled RC frames: an experimental study, Eng. Struct. 238 (2021/07/01/2021) 112258.
[20] R. Angel, D. Abrams, D. Shapiro, J. Uzarski, M. Webster, Behavior of Reinforced Concrete Frames, with Masonry Infills, Civil Engineering Studies, Reserach Series No. 589, UILU-ENG, Department of Civil Engineering, University of Ilinois, USA, 1994, 94-2005.

[21] M. Di Domenico, M.T. De Risi, P. Ricci, G.M. Verderame, G. Manfredi, Empirical prediction of the in-plane/out-of-plane interaction effects in clay brick unreinforced masonry infill walls, Eng. Struct. 227 (2021/01/15/2021) 111438.
[22] P. Ricci, M. Di Domenico, G.M. Verderame, Effects of the in-plane/out-of-plane interaction in URM infills on the seismic performance of RC buildings designed to eurocodes, J. Earthq. Eng. (2020) 1–35.
[23] M. Minotto, N. Verlato, M. Donà, F.d. Porto, Strengthening of in-plane and out-of-plane capacity of thin clay masonry infills using textile- and fiber-reinforced mortar, J. Compos. Construct. 24 (6) (2020) 4020059.
[24] S.L. Sagar, V. Singhal, D.C. Rai, In-plane and out-of-plane behavior of masonry-infilled RC frames strengthened with fabric-reinforced cementitious matrix, J. Compos. Construct. 23 (1) (2019) 4018073.
[25] M.T. De Risi, et al., Experimental analysis of strengthening solutions for the out-of-plane collapse of masonry infills in RC structures through textile reinforced mortars, Eng. Struct. 207 (2020/03/15/2020) 110203.
[26] A. Furtado, H. Rodrigues, A. Arêde, H. Varum, Experimental tests on strengthening strategies for masonry infill walls: a literature review, Construct. Build. Mater. 263 (2020). Art. no. 120520.
[27] J.L. Dawe, C.K. Seah, Out-of-plane resistance of concrete masonry infilled panels, Can. J. Civ. Eng. 16 (6) (1989) 854–864.
[28] M. Di Domenico, P. Ricci, G.M. Verderame, Experimental assessment of the influence of boundary conditions on the out-of-plane response of unreinforced masonry infill walls, J. Earthq. Eng. 24 (6) (2020) 881–919.
[29] Y.H. Tu, T.H. Chuang, P.M. Liu, Y.S. Yang, Out-of-plane shaking table tests on unreinforced masonry panels in RC frames, Eng. Struct. 32 (12) (2010) 3925–3935.
[30] D. Cardone, G. Perrone, Developing fragility curves and loss functions for masonry infill walls, En, in: Earthquakes and Structures, vol. 9, 07/25 2015, pp. 257–279, 1.
[31] M. Donà, M. Minotto, N. Verlato, F. da Porto, A new macro-model to analyse the combined in-plane/out-of-plane behaviour of unreinforced and strengthened infill walls, Eng. Struct. 250 (2022/01/01/2022) 113487.
[32] A. Furtado, H. Rodrigues, A. Arêde, H. Varum, Experimental evaluation of out-of-plane capacity of masonry infill walls, Eng. Struct. 111 (2016//2016).
[33] A. Furtado, H. Rodrigues, A. Arêde, J. Melo, H. Varum, The use of textile-reinforced mortar as a strengthening technique for the infill walls out-of-plane behaviour, Compos. Struct. 255 (2021). Art. no. 113029.
[34] M. Agante, A. Furtado, H. Rodrigues, A. Arêde, P. Fernandes, Experimental Characterization of the Out-Of-Plane Behaviour of Masonry Infill Walls Made of Lightweight Concrete Blocks 244, Engineering Structures, 2021.
[35] F. Akhoundi, G. Vasconcelos, P. Lourenço, Experimental out-of-plane behavior of brick masonry infilled frames, Int. J. Architect. Herit. 14 (2) (2018) 221–237.
[36] CEN, NP-EN 772-1 Métodos de ensaio de bolocos para alvenaria Parte 1: Determinação da resistência à compressão, 2002.
[37] CEN, EN 1052-1 Methods of Test for Masonry - Part 1: Determination of Compressive Strength, 1998.
[38] RILEM, RILEM TC 76-LUM. Diagonal Tensile Strength of Small Walls Specimens, RILEM Publications SARL, 1994.
[39] CEN, EN 1052-2: Methods of Test for Masonry, Determination of flexural strength, 1999.
[40] P. Ricci, M. Di Domenico, G.M. Verderame, Experimental investigation of the influence of slenderness ratio and of the in-plane/out-of-plane interaction on the out-of-plane strength of URM infill walls, Construct. Build. Mater. 191 (2018/12/10/2018) 507–522.
[41] M. Donà, M. Minotto, E. Saler, G. Tecchio, F. da Porto, Combined In-Plane and Out-Of-Plane Seismic Effects on Masonry Infills in RC Frames, vol. 34, Ingegneria Sismica, 2017, pp. 157–173. Special Issue.
[42] B. Pradhan, M. Zizzo, V. Sarhosis, L. Cavaleri, Out-of-plane behaviour of unreinforced masonry infill walls: review of the experimental studies and analysis of the influencing parameters, Structures 33 (2021/10/01/2021) 4387–4406.
[43] M. Di Domenico, P. Ricci, G.M. Verderame, Experimental assessment of the influence of boundary conditions on the out-of-plane response of unreinforced masonry infill walls, J. Earthq. Eng. (2018) 1–39.
[44] M. Griffith, J. Vaculik, N. Lam, J. Wilson, E. Lumantarna, Cyclic testing of unreinforced masonry walls in two-way bending, Earthq. Eng. Struct. Dynam. 36 (2007) 801–821.
[45] M. Di Domenico, P. Ricci, G.M. Verderame, Predicting the out-of-plane seismic strength of unreinforced masonry infill walls, J. Earthq. Eng. (2019) 1–38.
[46] A. De Angelis, M.R. Pecce, Out-of-plane structural identification of a masonry infill wall inside beam-column RC frames, Eng. Struct. 173 (2018/10/15/2018) 546–558.
[47] F. Colangelo, Drift-sensitive non-structural damage to masonry-infilled reinforced concrete frames designed to Eurocode 8, Bull. Earthq. Eng. 11 (6) (2013/12/01 2013) 2151–2176.
[48] A. Papasotiriou, A. Athanatopoulou, K. Kostinakis, Parametric study of the masonry infills' effect on the seismic performance of R/C frames based on the use of different damage measures, Eng. Struct. 241 (2021/08/15/2021) 112326.
[49] A. Rossi, P. Morandi, G. Magenes, A novel approach for the evaluation of the economical losses due to seismic actions on RC buildings with masonry infills, Soil Dynam. Earthq. Eng. 145 (2021/06/01/2021) 106722.
[50] A.H.A. da Silva, E.M.V. Pereira, G.L. Pita, G.H. Siqueira, L.C.M. Vieira Jr., Damage estimation in reinforced concrete buildings from induced earthquakes in Brazil, Eng. Struct. 234 (2021/05/01/2021) 111904.
[51] H. Hachem, J. Mahinand, P. Moehle, Performance of Circular Reinforced Concrete Bridge Columns under Bidirectional Earthquake Loading, 2003. *PEER 2003/06 - UCB/ENG-9374*.
[52] J.E. Stephens, J.T.P. Yao, Damage assessment using response measurements, J. Struct. Eng. 113 (4) (1987) 787–801.
[53] M.S. Williams, R.G. Sexsmith, Seismic damage indices for concrete structures: a state-of-the-art review, Earthq. Spectra 11 (2) (1995) 319–349.
[54] Y. Chung, C. Meyerand, M. Shinozuka, Seismic Damage Assessment of Reinforced Concrete Members, NCEER-87-0022, National Center for Earthquake Engineering Research, 1987.
[55] Y.J. Park, A.H.S. Ang, Mechanistic seismic damage model for reinforced concrete, J. Struct. Eng. 111 (4) (1985) 722–739.
[56] Eurocode 6, Part 1-1 – General Rules for Buildings – Rules for Reinforced and Unreinforced Masonry, European Committee for Standardisation, Brussels, 2005.
[57] Eurocode 8, Design of Structures for Earthquake Resistance - Part 1-1: General Rules, Seismic Actions and Rules for Buildings, B. European Committee for Standardization, Belgium, 2005.